A NUMERICAL STUDY ON THE DYNAMICS OF BUBBLE GROWTH AND DETACHMENT FROM AN ORIFICE

by

SHESHI KUMAR TAKKALLAPALLY

Presented to the Faculty of the Graduate School of

The University of Texas at Arlington in Partial Fulfillment

of the Requirements

for the Degree of

MASTER OF SCIENCE IN MECHANICAL ENGINEERING

THE UNIVERSITY OF TEXAS AT ARLINGTON

DECEMBER 2009

ACKNOWLEDGEMENTS

I would like to express my sincere gratitude to my supervising professor, Dr. Albert. Y. Tong, for his invaluable advice during the course of my research. I really appreciate his guidance and support. I enjoyed a lot working with him mainly because of his friendliness and patience. Whenever I was in need of some kind of help, he was always there. I have really learnt a lot from him as his student. He always tried to help me understand the problems in a better way and gave me ideas to overcome any sort of troubles. His idea of using analogies to make me understand the concept was really helpful. It is a great pleasure to work with Dr. Tong.

I would also like to thank my committee members, Dr. Dereje Agonafer and Dr. Hyejin R. Moon. I am really grateful for the assistantship provided by Mechanical and Aerospace Engineering Department at UTA. This provided me the financial security needed and helped me to concentrate on my research work.

Last but not least, I would like to thank my parents for their constant support, understanding and motivation. I am grateful for them for always helping me to choose the right path. I would also like to thank all my friends for their constant cooperation.

April 16, 2009

ABSTRACT

A NUMERICAL STUDY ON THE DYNAMICS OF BUBBLE GROWTH AND DETACHMENT FROM AN ORIFICE

Sheshi Kumar Takkallapally, M.S.

The University of Texas at Arlington, 2009

Supervising Professor: Albert Y. Tong

The study of bubble formation from an orifice finds numerous industrial applications which include bubble acoustics in ocean physics and chemical reactors. Numerical simulations have been performed to investigate the dynamics of bubble formation, growth and detachment from an orifice. The full transient Navier - Stokes equation is solved in a two-dimensional axi-symmetrical coordinate system. The surface tension implementation algorithm known as the Pressure Boundary Method (PBM) is used to model the surface tension. The robustness of PBM method on two-phase flows with different conditions has been shown. The results achieved by numerical simulations have been compared with the available experimental data for accuracy. Parametric studies have been done on the flow rates and inlet velocity profiles. The effect of fluid properties like density, surface tension, viscosity and gravity on bubble formation and growth has been studied. The conditions required for the formation of double-periodic bubbles have been emphasized. The physics of the bubble formation process has been

given. The results obtained in the present study are in good agreement with the experimental results provided in literature.

TABLE OF CONTENTS

LIST OF ILLUSTRATIONS

LIST OF TABLES

CHAPTER 1

INTRODUCTION

1.1 Objective

The accurate composition of two-phase problems has enormous importance in numerous scientific and industrial applications such as bubble acoustics in ocean physics and chemical reactors. In addition to these, controlled bubbling of gas into liquid is an essential part of genetic-engineering reactors, fermentation and waste water treatment.

The main objective of this study is to investigate the dynamics of bubble formation, growth and development from an orifice. Despite extensive studies on bubble formation, a fundamental understanding including the growth and development is lacking in the literature. The detachment of the bubble is a challenging process to observe because it occurs within a short period of time. The fluid variables such as velocity and pressure need to be tracked with a moving boundary and any kind of discontinuity makes the calculation challenging.

The correct simulation of flow behavior in a multi-fluid system depends on the ability to satisfactorily model the flow mechanism for each fluid phase as well as the interactions between them. While simulating two-phase flows, care has to be taken regarding the sharp interfaces which tend to produce discontinuities in fluid properties such as density and viscosity. Also with the presence of surface tension there would be a pressure jump across the interface.

In the present study a modified version of RIPPLE [1], which was originally developed at the Los Alamos National Laboratory, is used. The code is capable of modeling free surfaces especially flows with low accelerations and strong restoring forces such as surface tension force. It can handle transient, two-dimensional, incompressible flow and the free surfaces are represented with volume of Fluid (VOF) data on a fixed Eulerian grid. Over the past fifteen years substantial modifications have been made to this computer code by the researcher group at The

University of Texas at Arlington under the supervision of Professor Albert Y. Tong. These include the addition of an energy equation solver, implementation of various robust schemes such as piecewise linear interface construction (PLIC), coupled level set and volume-of-fluid (CLSVOF) and pressure boundary method (PBM).

Parametric studies have been done on the effect of inlet velocity profile, viscosity, gravity, and surface tension coefficient. Generally, it is not feasible to set the initial condition of numerical simulation identical to the experiment since the shape and velocity profile at a specific time cannot be accurately measured in the experiment. For this reason, successive bubble formation has also been studied to see the effect of initial condition on the bubble formation.

1.2 Organization of Thesis

A literature review on bubble formation process is presented in Chapter 2. Chapter 3 presents a brief description of the PBM algorithm with numerical formulation. The results obtained in the present study are discussed in Chapter 4. Comparisons with the results in the literature are reported. The conclusions drawn are provided in Chapter 5 along with the areas of work that can be carried in the future.

CHAPTER 2

BUBBLE FORMATION MECHANISM

2.1 Introduction

The process of bubble formation finds many industrial applications which operate on the basis of gas-liquid as the primary media. In order to design any apparatus for such uses care has to be taken in maintaining an accurate knowledge about the size of the bubble. Proper understanding about the operating conditions is very important. The experimental results reported by Manasseh et al. [2] provide a good understanding of the various industrial applications. They monitored the acoustic signals emitted on bubble formation which finds application in tools for bubble sizing used in biotechnology, ocean physics, etc. Many studies have been done and reported in the literature about bubble formation at an orifice. Experimental studies were done by Zhang and Shoji [3] to observe the process of bubble formation, detachment and growth. They published photographs showing successive bubble formation and growth which were later examined by Gerlach et al. [4] using numerical methods in which a qualitative analysis of bubble formation and growth was also provided. Their numerical results were reported to be in good agreement with the experimental data. Prior to these, there were many theoretical approaches to study the problem of bubble formation. Kumar and Kuloor [5], Clift et al. [6], Tsuge [7], Kulkarni and Joshi [8], are few to name. Longuet-Higgins et al. [9] made analytical predictions for bubble contour using balance of pressure and capillary forces. The experimental work on bubble formation and growth can be divided into two categories, one which concentrates primarily on a single bubble formation and growth as reported by Davidson and Schuler [10, 11] and the second which concentrates on interactions between successive bubble formation as shown by Zhang and Shoji [3].

In the work done by Zhang and Shoji [3], the concentration was primarily on observing the relation between bubble behaviors and aperiodic characteristics of bubble detachment at a submerged orifice for a wide range of air flow rate. The data obtained by them were in agreement with the theoretical results published in the literature.

The numerical results reported by Gerlach et al. [4] used a combination of volume-of-fluid and level-set methods. A single set of Navier-Stokes equations in an axisymmetric formulation was solved in the computational domain. They produced results on the effect of various parameters which include radius of orifice, flow rates, wettability of orifice material and fluid properties such as surface tension, liquid density and viscosity.

The present numerical study is similar to what has been done by Gerlach et al. [4] as far as the scope of work is concerned. However the difference lies in the velocity profile. The current study uses a uniform velocity profile while the one reported in Gerlach et al. [4] uses a parabolic velocity profile. The present work includes single bubble formation, multiple bubble formation and the transition of formation regime from periodic to Double-periodic. This pattern was observed experimentally by Kyriakides et al. [12], Zhang and Shoji [3] and Tufaile and Sartorelli [13]. In these studies, the flow rates were increased in a stepwise pattern to observe the transition. In the present study variation of surface tension coefficient has been considered to produce the transition from single-periodic to double-periodic. Gerlach et al. [4] varies both the flow rate and the surface tension coefficient to study the transition from single-periodic to double-periodic regime. According to Gerlach et al. [4], in a double-periodic regime the influence of a leading bubble on the trailing one is such that the second one detaches sooner when compared to a periodic regime and the size of the trailing bubble is smaller than the leading bubble and two distinct time-periods which remain constant exist.

2.2 Bubble formation mechanism

Bubble formation and rise is a good example of a two-phase problem. The volume of the bubble increases when the fluid (air) flowing through the nozzle rises. When the opposing

forces (viscous and capillary forces) are overcome by the lift forces, the bubble detaches and starts to rise.

2.2.1 Bubble Formation

According to Zhang and Shoji [3], bubble formation is assumed to take place in two stages—the expansion stage and the elongation stage.

2.2.1.1 Expansion stage

In this stage the bubble grows radially due to the inflowing gas (air), but the base of the bubble is attached to the orifice. This process continues until the opposing forces start to dominate the lifting forces. The expansion stage comes to an end when the opposing forces become equal to or larger than the lifting forces.

2.2.1.2 Elongation stage

Additional amount of gas is fed into the bubble through the orifice which results in further growth of bubble size. The bubble starts to lift off from the orifice but still is attached to it via a neck. This neck also starts to grow with time. After a certain period of time the neck becomes very thin and pinches off thereby causing the bubble to detach. According to Kim et al. [14], the bubble neck is assumed to collapse when the neck length becomes larger than or equal to the orifice diameter.

2.2.2 Bubble Detachment and Ascendance

When the neck pinches off suddenly, the force balance of the bubble which was present gets disturbed as some of the forces vanish. We can observe that the upper part of the detached bubble maintains its shape and position due to inertia, but the lower part shrinks towards the bubble center. After detachment the balance of forces on the bubble is maintained by interactions with surrounding liquid. Buoyancy force, inertia force and drag forces are considered to be the major forces exerted on the detached bubble.

2.2.3 Bubble Interference

In the periodic regime, the wake velocity of a leading bubble has negligible effect on the successive bubble as the distance between them is too large. However when the distance between the bubbles becomes shorter due to higher flow rates interference of leading bubble with the next occurs. As a result there is a significant change in the shape of the bubble. The wake effect of the leading bubble causes the trailing bubble to deform in the vertical direction changing the shape of the bubble from spherical to ellipsoidal when interference occurs.

2.2.4 Bubble Collision

A transition exists between bubble interference and bubble coalescence when the trailing bubble contacts and collides with the leading bubble. During collision the trailing bubble is ellipsoidal in shape similar to the one in interference condition. The two bubbles only collide without coalescence when the collision force of the trailing bubble is less than the surface tension force of the leading bubble.

2.2.5 Bubble Coalescence

With the increase in gas flow rate, the collision force of trailing bubble becomes larger than surface tension of leading bubble thus causing both the bubbles to coalesce. Bubble coalescence is further divided into two conditions:

i) Bubble coalescence in expansion stage. The trailing bubble again deforms when the coalescence of the bubbles occur in the expansion stage of trailing bubble. After coalescence both bubbles start to rise with constant velocity.

ii) Bubble coalescence in elongation stage. The trailing bubble is not assumed to deform if the bubbles coalesce in the elongation stage of trailing bubble. They rise with common velocity after coalescence.

The coalesced bubble rising is termed as double bubble. As the flow rates increases further, this double bubble interferes, collides or coalesces with the trailing bubbles.

The bubble formation process described in Zhang and Shoji [3] mainly discuss about the trailing bubble colliding and coalescing with the leading bubble at the orifice. Similar kind of pattern exists after the leading bubble rises to certain extent and the trailing bubble reaches it.

CHAPTER 3

NUMERICAL FORMULATION

3.1 Basic Equations

Away from the interface, the continuity and Navier-Stokes equations for incompressible flows are given by:

$$\nabla \bullet \vec{V} = 0 \tag{3-1}$$

$$\frac{\partial \vec{V}}{\partial t} + \nabla \bullet (\vec{V}\vec{V}) = -\frac{1}{\rho}\nabla p + \frac{1}{\rho}\nabla \bullet \tau + \vec{g} \tag{3-2}$$

where $\vec{V}$ is the velocity, ρ the density, p the pressure, τ the viscous stress tensor, and $\vec{g}$ the gravitational acceleration. The stress tensor, τ , for Newtonian fluids can be written as

$$\tau = 2\mu S \tag{3-3}$$

where μ is the dynamic viscosity and S is the strain rate tensor given by:

$$S = \frac{1}{2}[(\nabla \vec{V}) + (\nabla \vec{V})^T] \tag{3-4}$$

Equation (3-2) is discretized as:

$$\frac{\vec{V}^{n+1} - \vec{V}^n}{\delta t} = -\nabla \bullet (\vec{V}\vec{V})^n - \frac{1}{\rho^n}\nabla p^{n+1} + \frac{1}{\rho^n}\nabla \bullet \tau^n + \vec{g}^n \tag{3-5}$$

where the superscripts n and n+1 represent the value of the variable at consecutive time steps. Pressure is the only implicit term in the above equation while gravity, advection and viscosity are approximated with old time t^n values. Equation (3-5) is solved using a two-step projection method by decomposing it into two equations and solving them consecutively. In the present study, the surface tension effect is treated as pressure jump condition. The projection method in

conjunction with the surface tension implementation algorithm, referred to as pressure boundary method (PBM) will be discussed in later sections.

3.2 Free surface tracking

In the present study two Eulerian based methods namely volume of fluid (VOF) [15-19] and level set (LS) [20] methods are used to track the free surfaces. These methods have the advantage of handling flow problems involving large topological changes and interface deformations such as bubble growth, rise and detachment with ease.

In the VOF method, free surfaces are reconstructed using a scalar field, F, known as VOF function and is defined as:

$$F(\vec{x},t)=\begin{cases}1, & \text{in the fluid,}\\ 0<\mathrm{F}<1, & \text{at free surface,}\\ 0, & \text{external to fluid.}\end{cases} \tag{3-6}$$

from the above definition it can be inferred that VOF function represents non-dimensional density of fluid in a cell.

The LS function, ϕ, is a distance function whose magnitude equals the shortest distance from the interface and its sign determined as:

$$\phi(\vec{x},t)\begin{cases}>0, \text{outside of the interface,}\\ =0, \text{at the interface,}\\ <0, \text{inside the interface.}\end{cases} \tag{3-7}$$

The VOF and LS functions are advanced by the following equations:

$$\frac{DF}{Dt}=\frac{\partial F}{\partial t}+(\vec{V}\bullet\nabla)F=0 \tag{3-8}$$

$$\frac{D\phi}{Dt}=\frac{\partial \phi}{\partial t}+(\vec{V}\bullet\nabla)\phi=0 \tag{3-9}$$

It can be observed that VOF function is not smoothly distributed at the free interface so an interface reconstruction procedure is required to evaluate the VOF flux across the cell with a

free surface. In the present study, the interface is reconstructed via a PLIC scheme [19] and the LS function is used to calculate the interface normal given by:

$$\hat{n} = \frac{\nabla \phi}{|\nabla \phi|} = \nabla \phi \tag{3-10}$$

After the LS function is advanced by Equation (3-9), it fails to be a distance function and a re-initialization process [20] is needed. It is achieved by solving the following re-initialization equation:

$$\frac{\partial \phi}{\partial t} = \frac{\phi_0}{\sqrt{\phi_0^{\,2} + h^2}} (1 - |\nabla \phi|) \tag{3-11}$$

where ϕ_0 is the LS function of the previous time step, *t* the artificial time, and *h* the grid width. The local curvature of the free surface interface can be computed directly from the LS function as:

$$\kappa = \nabla \bullet \nabla \phi \tag{3-12}$$

The LS function is a smooth function when compared to the VOF function which is a jump function. Thus it is expected that LS function would show a better accuracy while calculating the gradient of the function.

3.3 Pressure Boundary Method

In the present study, the surface tension implementation algorithm known as pressure boundary method (PBM) is used. This algorithm was developed by Wang [21]**.** In this method the surface tension effect which is discontinuous across the interface is treated as a sharp boundary condition at the interface for a capillary pressure field. The surface tension force is incorporated into the Navier-Stokes equation via a pressure gradient term. The other discontinuous properties at the interface, such as density and viscosity, however, are treated in a continuous way and given as:

$$\rho = \rho_g (1 - F) + \rho_l F \tag{3-13}$$

$$\mu = \mu_g (1 - F) + \mu_l F \tag{3-14}$$

for free surface flows, both ρ_g and μ_g are zero.

Both density and viscosity are weighed by the VOF function, *F.* As a result more accurate estimation of the density and viscosity at the interfacial cells would be possible also allowing mass conservation to be well preserved. On the other hand, the smearing of the density and viscosity can prevent disturbances resulting from the otherwise sharp treatment [22].

3.3.1 PBM Algorithm

As stated earlier, in the PBM method the surface tension force is incorporated into the Navier-Stokes equation via a pressure gradient term. The pressure term in Eq. (3-5) is separated into two components: one accounts for the surface tension and the other for achieving mass conservation. The surface tension induced sharp pressure conditions at the free surface are satisfied by the pressure field obtained.

Primarily, a capillary pressure field, p_1, is computed from the following equation:

$$\nabla \bullet \left[\frac{1}{\rho^n} \nabla p_1 \right] = 0 \tag{3-15}$$

with the jump boundary condition due to surface tension at the free surface applied. More about the discretization of this boundary condition based on the technique described by Gibou et al. [23] will be presented in the following section.

Next, the momentum equation given by Eq. (3-5) is decomposed into the following two equations using the two-step projection method [1]. The two equations are:

$$\frac{\vec{\tilde{V}} - \vec{V}^n}{\delta t} = -\nabla \bullet (\vec{V}\vec{V})^n + \frac{1}{\rho^n} \nabla \bullet \tau^n + \vec{g}^n - \frac{1}{\rho^n} \nabla p_1 \tag{3-16}$$

$$\frac{\vec{V}^{n+1} - \vec{\tilde{V}}}{\delta t} = -\frac{1}{\rho^n} \nabla p_2 \tag{3-17}$$

where $\vec{\tilde{V}}$ represents an intermediate velocity and $\vec{V}^n$ is the velocity from the previous time step.

In the first step of the projection method, an intermediate velocity field $\vec{\tilde{V}}$ is computed from Eq. (3-16). However $\vec{\tilde{V}}$ will not satisfy the continuity equation. Therefore we take the divergence of Eq. (3-17) while imposing the incompressibility condition on the velocity field $\vec{V}^{n+1}$ with:

$$\nabla \bullet \vec{V}^{n+1} = 0 \tag{3-18}$$

We obtain the following single Poisson equation:

$$\nabla \bullet \left[\frac{1}{\rho^n} \nabla p_2 \right] = \frac{\nabla \bullet \vec{\tilde{V}}}{\delta t} \tag{3-19}$$

solving the Poisson Equation, Eq. (3-19) using an incomplete Cholesky conjugate gradient solution technique we can obtain pressure p_2. The velocity field $\vec{V}^{n+1}$ is then updated via Eq. (3-17) and pressure p^{n+1} from:

$$p^{n+1} = p_1 + p_2 \tag{3-20}$$

A flow chart for the overall computational cycle is given in Figure 3.1.

3.3.2 Capillary Pressure Field Calculation

The capillary pressure field is obtained by solving Eq. (3-15) with a Dirichlet boundary condition. Discretization of Equation (3-15) gives:

$$\frac{(\nabla p_1 / \rho)_{i+1/2,j} - (\nabla p_1 / \rho)_{i-1/2,j}}{\Delta x} + \frac{(\nabla p_1 / \rho)_{i,j+1/2} - (\nabla p_1 / \rho)_{i,j-1/2}}{\Delta y} = 0 \tag{3-21}$$

At the interface, the complete pressure jump condition is given by

$$p - p_v = \sigma\kappa + 2\mu n_k \frac{\partial u_k}{\partial n} \tag{3-22}$$

Both the surface tension and viscous stress at the interface contribute to the pressure jump. Since p_1 is extracted to handle the surface tension effect only, the pressure jump condition for solving Equation (3-22) is reduced to the Laplace's formula:

$$p - p_v = \sigma\kappa \tag{3-23}$$

where p_v is the vapor (or gas) pressure. The dynamic effect of one phase (e.g., gas) is neglected for free surface flows, where the pressure is treated as constant. Thus, the jump pressure condition becomes a Dirichlet boundary condition at the interface given by:

$$p_I = p_v + \sigma\kappa \tag{3-24}$$

the liquid side interface pressure, p_I, is used as the boundary value for p_1 in the solution of Eq. (3-21).

To discretize Eq. (3-15) with boundary condition (3-24) the method used in [23] is used. With reference to Figure 3.2, the pressure gradients in Eq. (3-21) at the faces of cell (i, j) are given by:

$$(\nabla p)_{i+1/2,j} = \frac{p_{Ir} - p_{i,j}}{\theta_r \Delta x} \tag{3-25a}$$

$$(\nabla p)_{i-1/2,j} = \frac{p_{i,j} - p_{i-1,j}}{\Delta x} \tag{3-25b}$$

$$(\nabla p)_{i,j+1/2} = \frac{p_{It} - p_{i,j}}{\theta_t \Delta y} \tag{3-25c}$$

$$(\nabla p)_{i,j-1/2} = \frac{p_{i,j} - p_{i,j-1}}{\Delta y} \tag{3-25d}$$

where p_{Ir} and p_{It} are pressures at the interface which can be obtained from Eq. (3-24). θ is the fraction of the distance from the interface to the center of cell (i, j) given by (refer to Figure 3.2):

$$\theta_r = \frac{\left|\phi_{i,j}\right|}{\left|\phi_{i,j}\right| + \left|\phi_{i+1,j}\right|}$$
$$\theta_t = \frac{\left|\phi_{i,j}\right|}{\left|\phi_{i,j}\right| + \left|\phi_{i,j+1}\right|} \qquad (3\text{-}26)$$

with the LS function, ϕ, serving as the distance function.

The level set function which is a sign function is used to locate the free surface where its value changes sign and the discretization given in Eq. (3-13a) and Eq. (3-13c) are applied. Otherwise, standard discretization given in Eq. (3-13b) and Eq. (3-13d) are used. The same discretization procedure should be followed when approximating pressure gradients in Eq. (3-16) and this is essential to maintain balance between surface force and pressure gradients. Eq. (3-15) takes the following form after discretization:

$$\nabla \bullet \left[\frac{1}{\rho}\nabla p\right]_{i,j} = \frac{(\nabla p/\rho)_{i+1/2,j} - (\nabla p/\rho)_{i-1/2,j}}{\Delta x} + \frac{(\nabla p/\rho)_{i,j+1/2} - (\nabla p/\rho)_{i,j-1/2}}{\Delta y} = 0 \qquad (3\text{-}27)$$

which can be readily solved using an incomplete Cholesky conjugate gradient (ICCG) method [24]. It can be observed that although density is constant for incompressible fluids, it is retained inside the divergence operator. By treating density as a variable at the free surface, better grid convergence with reduced numerical errors can be achieved.

For two-phase interfacial flows, if no interface exists between two adjacent cells, the standard discretization method can be used to approximate the pressure gradient at the cell face. On the other hand, special attention must be paid to the discretization of the derivative at the cell face if an interface exists between two adjacent cells, because pressure is not continuous across the interface due to the jump conditions induced by the surface tension effect, the standard discretization method described above cannot be applied; otherwise, the pressure profile will be numerically smeared as in the continuum method.

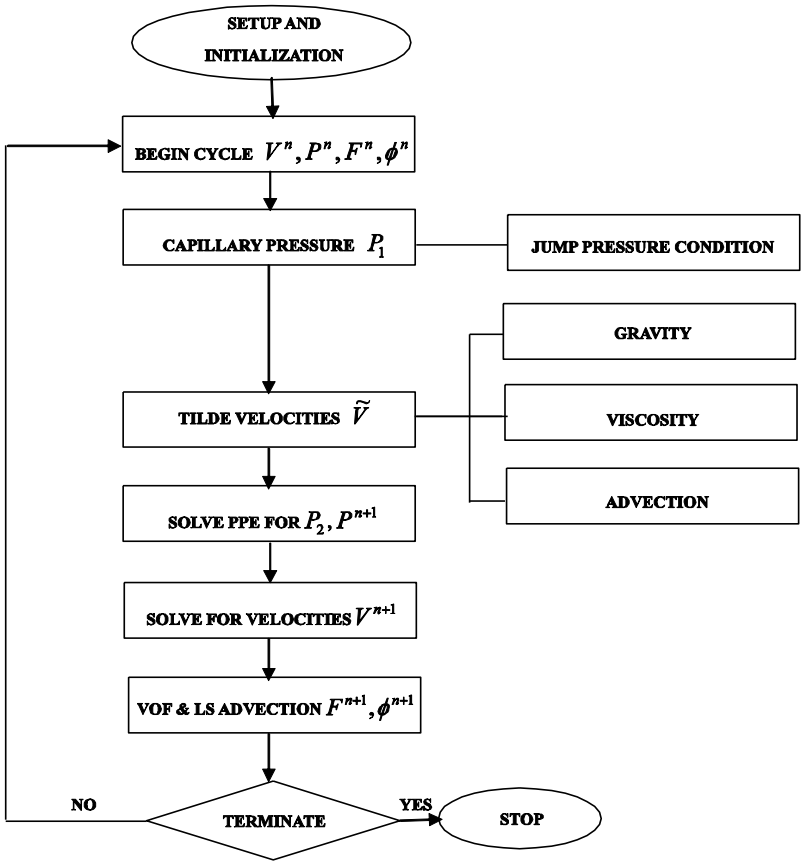

Figure 3.1 Flowchart for one computational cycle [21]

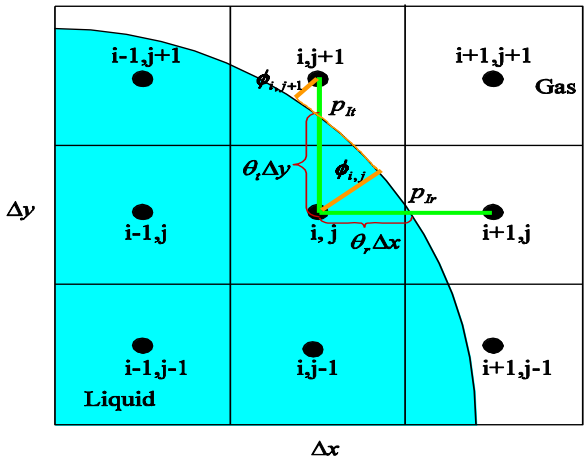

Figure 3.2 Discretization of pressure gradient at the interface and determination of the distance fraction θ [21].

CHAPTER 4

RESULTS AND DISCUSSION

4.1 Introduction

This chapter is divided into two sections. The first section emphasizes more on single periodic bubble formation and growth. A standard case is defined and the results obtained are compared with published experimental data. This is done to demonstrate the validity of the numerical scheme. Several parametric studies have been done to examine the effect of inlet velocity profile, fluid parameters and gravitational acceleration on bubble formation, growth and detachment. The second section describes the phenomenon of multiple bubbles. Here the concepts of double-periodic and triple-periodic bubble formation are explained. The numerical computation carried out in this study solves the full transient Navier-Stokes equation in a 2D axi-symmetrical coordinate. Air and Water at 20^{o}C are the working fluids and the physical properties are given in Table 4.1.

Table 4.1 Properties of the Reference Fluid: Air-Water (aw) System at 20^{o}C

Property	Unit	Value
Kinematic viscosity of air	mm^2/ms	1.51×10^{-2}
Kinematic viscosity of water	mm^2/ms	1.005×10^{-3}
Density of air	g/mm^3	0.99
Density of water	g/mm^3	1.2×10^{-3}
Surface Tension Coefficient	N/m	7.27×10^{-2}

The initial and boundary conditions are prescribed such that comparisons can be made with experimental and numerical results available in the literature [4]. The computational domain

in cylindrical coordinates is shown in Figure 4.1. An orifice is inserted as an obstacle in the computational domain.

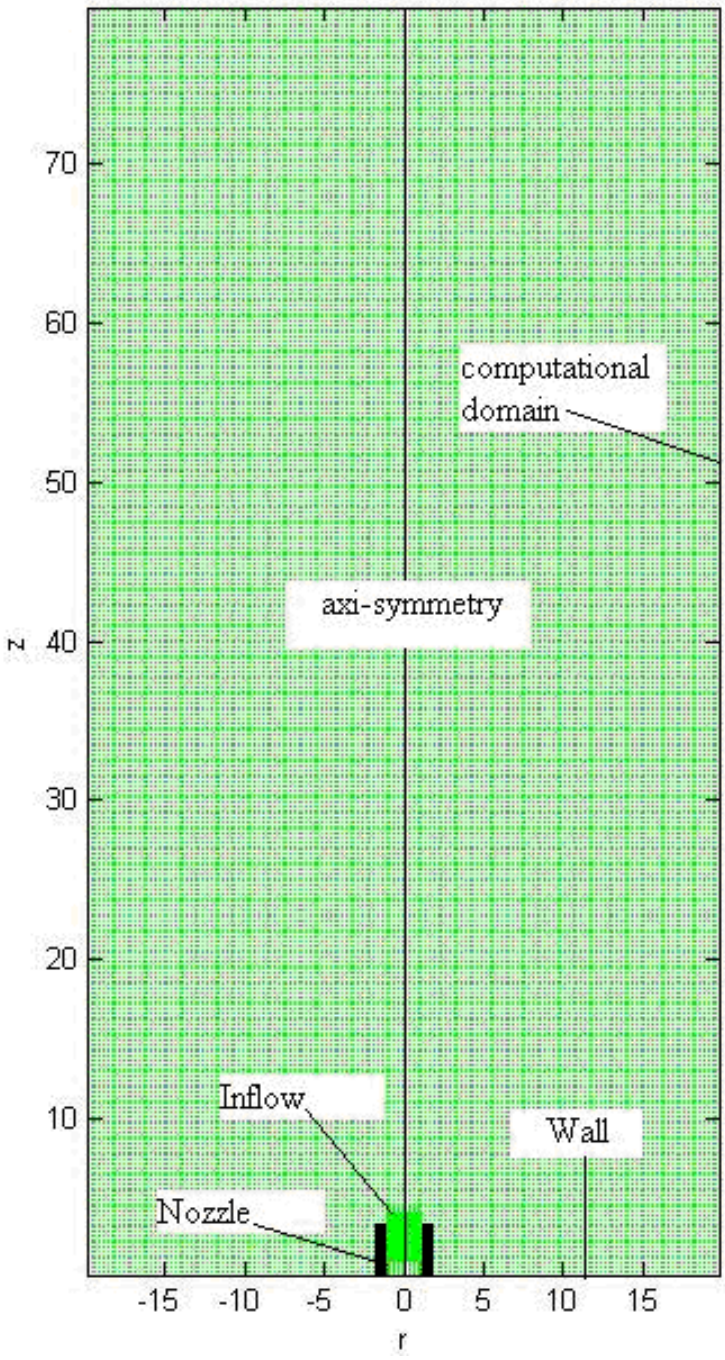

Figure 4.1 Computational domain and boundary conditions.

Axi-symmetric calculation is performed to conserve computational resources. No-slip condition is maintained at the inner wall of the orifice i.e. $v_r = v_z = 0$. The fluid is initially at rest. As shown in Figure 4.1, the initial shape of the free surface is flat across the whole front surface. Figure 4.2 shows a schematic of a bubble rising from the orifice.

4.2 Convergence Study

Three time step constraints are used in the computer code for stability [1], they are viscous, courant and capillary conditions. The time step is adjusted accordingly using these conditions in the code. However the adjusted time step does not guarantee the accuracy of calculation especially for flows involving strong capillary effect. It is only sufficient to maintain stability. Accurate results can be obtained by reducing the *dtmax* parameter in the *input* file. This parameter denotes the maximum time step allowed for calculations.

In order to validate the numerical results, convergence study has been done. The results of time convergence study with grid sizes of 0.1mm and 0.25mm is shown in Table 4.2. The values of bubble detachment time, t^*, converges as *dtmax* is reduced. Though we cannot compare the two grid sizes directly, we have the non-dimensional characteristic values which are almost identical. This suggests that the solution is converging.

Table 4.2 Time Convergence Study

dtmax [ms]	t*[ms] with dr= dz= 0.1mm	t*[ms] with dr= dz= 0.25mm
8.28e-3	41.15	41.32
4.14e-3	42.29	41.99
2.93e-3	42.50	41.99
1.47e-3	42.67	42.33

Considering accuracy and computational limitation, the grid size of dr = dz = 0.25 mm has been adopted with *dtmax* = 4.14 x 10^{-3} *m*s. A 20mm (Width) X 80mm (Height)

computational domain is used for all simulations. Simulations have been performed to determine the optimum size of the domain. The domain size chosen follows the guidelines for dimensions provided in the literature [4]. Multiple simulations were performed to determine the optimum width of the domain. The width is chosen in such a way that the bubble formation process is unaffected by the lateral boundaries. Care has been taken regarding the height of the domain in a way that the bubble dynamics above the orifice are not influenced by the outflow boundary conditions [4]. The height of the domain is chosen in order to enable the observation of multiple bubbles. With adequate height it would be possible to capture the rise and interaction of successive bubbles.

4.3 Breakup Mechanism

The pressure distribution of the bubble at the instance of pinch-off is shown in Figures 4.3 and 4.4. The bubble is formed just above the conical region. The pressure along the gas (air) bridge is higher than that of the bubble and the conical region. It can be observed from the Laplace's formula given in Eq. (3-23) that the pressure at the interface is proportional to the curvature. The gas (air) bridge region has higher pressure due to larger radial curvature compared to the conical and bubble region. The pressure gradient in the z-direction causes the flow to be squeezed out of the gas (air) bridge which results in bubble pinch off. Velocity is increased at the neck and becomes largest causing the mass flow rate of this region to be quite large. The large amount of mass flowing in along with the pressure gradient along z-axis causes the bubble to detach. A large pressure variation can be observed at the tip of the gas (air) bridge at the instant of pinch-off in Figures 4.3 and 4.4. Figures 4.5 - 4.7 show the magnified velocity profiles at the instant of bubble detachment. Figure 4.5 shows the shape of the bubble just before detachment. At this instant though large pressure gradient in the z-direction is present as shown in Figure 4.3, no pinch-off is observed. This is because the mass flow rate is not sufficient to bring a detachment. As the mass flow rate increases the bubble detaches from the neck as shown in Figure 4.6. A large downward velocity can be observed in Figure 4.7

which is due to the large curvature at the tip which results in fast recoiling flow. The mechanism behind the formation of the trailing bubbles is similar to that of the leading bubble in the case of periodic bubble formation. However for the double-periodic case the formation of the trailing bubble is influenced by the wake effect of the leading bubble thus causing it to detach earlier and the two bubbles rise in tandem. The streamline profile and the velocity profile of the bubbles rising are shown in Figures 4.8 – 4.9. In Figure 4.8, the streamline and velocity profiles of the leading bubble can be observed while Figure 4.9 shows the profiles for the successive bubbles.

4.4 Influence of Operating Conditions

The effect of fluid flow rate Q, and the orifice material φ_s (wettability) on the bubble formation process were examined. The fluid properties were kept constant at reference values of air-water system at 20^{o}C. The radius, height and thickness of the orifice are 1mm, 3mm and 0.1 mm respectively.

4.4.1 Orifice Material

The influence of wettability ($\varphi_{s,}$ static contact angle) of the orifice material on the bubble formation process is examined. In this we study the effect of orifice material through the contact angle made by the liquid–vapor interface at the bubble base with the wall. Two contact angles are observed during the bubble formation and growth. They are static contact angle, $\varphi_{s,}$ which depends on the liquid, vapor and material of the solid surface and the dynamic contact angle, $\varphi_{,}$ which varies during the bubble formation and growth. The effect of orifice material can be studied either by defining a static contact angle or by defining a constant advancing and receding contact angles [25]. In the present study the static contact angle was varied to examine the influence of orifice material. It is assumed that if $\varphi_s > 100^0$ it is non-wetting liquid and if $\varphi_s < 50^0$, it is considered as wetting liquid. It has been shown in literature [4] that the dynamic contact angle φ at the bubble base has large values at the instant of detachment. For higher φ_s the bubble base widens and spreads along the orifice surface at the top and in a contrasting manner if φ_s is small then the base of the bubble remains at the orifice. In this

situation, the bubble volume at detachment is governed by the outer radius of the orifice. With an increase in $\varphi_{s,}$ the maximum bubble base diameter attained also increases which results in an increase in capillary forces acting downward leading to a rise in bubble volume. It has been reported in the literature that when $\varphi_s > 100^0$, the volume of the bubble V_B is roughly three times larger than when $\varphi_s < 50^0$. This suggests that in order to predict the volume of the bubble detached, the influence of orifice material should be considered. However the results obtained in the present study were not in support of those provided in the literature [4]. No significant change in bubble volume was observed. The reason for this could be the orifice thickness.

4.4.2 Orifice Flow Rate

The bubble formation for different flow rates has been studied. All the other parameters were kept constant. Evolution of bubbles with different flow rates is shown in Figure 4.10. It has been reported in literature [4] that the flow rate Q has a significant influence on the detachment time, t^* and the detached volume, V_B. For very low flow rates (1-10 ml/min), t^* is independent of flow rates. At higher flow rates (>100 ml/min) the frequency at which the bubbles are formed increases but the volume of the bubble remains constant. In the present study stress has been laid on understanding the bubble formation behavior for the flow rates between 10-100 ml. However in the present study, with the restriction of the computer code's inability to solve the high flow rate problems, attention was paid to flow rates between 50-100 ml/min. The detachment times obtained from numerical simulations in the present study for various flow rates are provided in Table 4.3.

Table 4.3 Bubble Detachment Times for Various Flow Rates.

Flow rate (ml/min)	t* (ms)
50	59.5
80	42.5
100	41.99

4.5 Influence of Fluid Parameters

4.5.1 Effect of Inlet Velocity Profile

Two velocity profiles, parabolic and uniform are compared to observe the influence of velocity profile on the bubble formation. All other parameters including the flow rate Q are unchanged. The bubble formation sequence is shown in Figure 4.11. In this the sub figures correspond to the level of the evolution relative to the detachment time, t*. With a parabolic profile, the bubble detachment occurs at about 2ms earlier compared to uniform profile. The volume of the fluid entered in a uniform flow is slightly larger than the one with parabolic flow. This is because in a parabolic profile, the flow is more centrally distributed than that in uniform case. With the amount of mass being preserved, the volume of bubble becomes higher. There is not much difference in detachment times between successive bubbles (i.e., $t_2^* - t_1^*$). This shows that effect of inlet velocity profile is negligible. Also there is no significant variation in bubble formation sequence between the parabolic and uniform velocity profiles.

4.5.2 Effect of Density

In this section, we investigate the effects of the liquid density on bubble formation process. For this the liquid density is varied keeping all other parameters constant. When the liquid density is increased, the buoyant force increases for a given bubble volume while surface tension is assumed to remain constant. From the equation provided by D. Gerlach et al.[4], to find the volume at detachment V_B using the balance of buoyancy and surface tension forces,

$$2\pi R\sigma \approx V_B (\rho_l - \rho_g) g \qquad (4\text{-}1)$$

where g = gravitational acceleration, we can say that the bubble volume decreases for increasing liquid density. This phenomenon can be observed in Figure 4.12, where the bubble volume decreases with increase in liquid density. For convenience the four figures have been overlapped for better view. Bubble-detachment time, t*, for various densities is shown in Table 4.4. In the current study, three different values for liquid density have been tested. The three values of liquid density used are 0.25, 1.25 and 1.50 times the reference value (ρ_l = 1.00 in

Table 4.4). It was observed that with increase in liquid density, the time for bubble detachment is gradually reduced.

Table 4.4 Time of Bubble-Detachment, t^*, for Various Densities

Liquid density, ρ_l [kg/m^3]	t^*[ms]
0.25	116.8
1.00	41.99
1.25	40.29
1.50	37.91

4.5.3 Effect of Liquid Viscosity

The relation between liquid viscosity, flow rates, surface tension effect and orifice radius can be understood from the definition of capillary number. The capillary number or the ratio of viscous to capillary forces is proportional to viscosity and orifice flow rates. For very low flow rates the only forces acting are capillary and buoyancy forces and the effect of viscosity is negligible. In the simulations, keeping all the fluid parameters but the liquid phase viscosity constant, we investigate the effect of viscosity alone on the bubble pinch-off.

In the present study the effect of the dimensionless liquid viscosity, v/v_{ref} on the formation of bubble was examined. Detachment times for different viscosities are presented in Table 4.5. The detachment time gradually increases with increase in the ratio. When the dimensionless liquid viscosity number was varied from 0.1 to 1, very little increase in detachment times was observed. No significant variation in detachment times was observed for values from 1 to 150. However when this value was increased to 150, the formation time was about doubled. The high liquid viscosity tends to retard the bubble pinch-off process. As a result more gas is accumulated in the bubble resulting in increase in the volume. Thus the bubble formation time is increased. It can be observed from Figure 4.13 that the bubble volume is minimal for low viscosities while it is large for high viscosities. The other factor to be observed is

the shape of the bubble. The bubble formed when the liquid has higher viscosity is more spherical than the other cases. Figure 4.13(c) shows a strange behavior of bubble for higher viscosities. Though the top half of the bubble is more spherical, the bottom of the bubble is elongated vertically before it detaches from the neck. As a result the detachment time is increased. The attached bubble is elongated in vertical direction for higher viscosity liquids. From the equation provided by Wong et al. [26], for the time for the neck to pinch off:

$$t_n = 7.6\frac{\mu_{l,aw} R_o}{\sigma_{aw}} \tag{4-2}$$

where R_0 is the radius of the orifice, we can clearly observe that the pinch-off time is directly proportional to the viscosity of the liquid. There is not much difference between the bubble shapes for $v/ v_{ref} < 1$.

Table 4.5 Detachment Times for Different Viscosities

v / v_{ref}	t^* (ms)
0.1	41.65
1.0	41.99
150	109.3

4.5.4 Effect of Surface Tension

Surface tension is one of the major factors affecting the bubble formation. To examine the surface tension effect, the magnitude of surface tension coefficient, σ, is varied from 0.41 to 2.75 times the reference value while other parameters are kept constant. The detachment times, t*, for different values of σ are provided in Table 4.6. It can be observed from Equation (4-1), that the bubble volume is related to surface tension. Surface tension significantly affects the pinch-off and there by the bubble volume. The bubble volume increases if surface tension is increased which causes a delay in the detachment time. It is observed that for the values of σ

less than 0.60 times the reference values, the detachment mechanism changes from periodic to a double-periodic regime. This can be observed in Figure 4.14. An effective control on surface tension has the stabilizing influence on the bubble formation process. The double-periodic regime can be transformed to a periodic regime by increasing the surface tension. When the surface tension is increased, the bubble volume is increased which in turn reduces the successive bubble interaction. One way of reducing the influence of surface tension is by increasing the flow rates.

Table 4.6 Detachment Times for Different Surface Tension Coefficient Values

σ (N/m)	t^* (ms)
3.635×10^{-2}	38.42
7.27×10^{-2}	41.99
19.99×10^{-2}	80.07

4.5.5 Effect of Gravity

Effect of gravitational acceleration is another area to observe while studying the bubble formation process. The magnitude of gravitational acceleration is varied to study its effect on bubble formation. When the magnitude is increased by a factor of 10 i.e., $g/g_s = 10$, the volume of the leading bubble formed is significantly reduced. The time for detachment is also significantly reduced. As a result for a given period of time the number of bubbles formed is more when compared to other cases. The size of bubble is also quite small. If we reduce the gravitational acceleration by a factor of 10 i.e., $g/g_s = 0.1$, then the volume of the leading bubble increases to a greater extent. It takes nearly 312ms for the leading bubble to detach. The shape of the bubble is also more like a perfect sphere. Figure 4.15 (a)–(c) show the successive shapes of bubbles for $g/g_s = 10$, 1.0 and 0.1 respectively. From the above study it is evident that magnitude of gravitational acceleration plays a key role in controlling the bubble formation process.

4.6 Modes of bubble formation

The main focus of present study is to concentrate on periodic bubble formation. However there are some instances where we observe the transition from periodic to double periodic. In a double periodic regime two distinct but constant detachment periods exist which repeat regularly. The double periodic regime was observed experimentally by Zhang and Shoji [3], Kyriakides et al. [12], and Tufaile and Sartorelli [13]. Gerlach et al. [4] later examined the results numerically. In a double periodic bubble formation, the detachment and rise of the leading bubble has a significant influence of the trailing bubble, causing it to detach earlier. As a result the volume of leading bubble becomes larger than the trailing bubble in each pair. The bubbles rise in pairs and coalesce at some height.

In literature [4], the concept of double periodic bubble formation was explained based on detachment time as a function of the required height the leading bubble has to rise to reduce the wake effect on the trailing bubble. They assumed that the leading bubble influences the trailing or forming bubble if the formation time T_2, of the trailing bubble is of the order of the time $T_{1,rise}$, which the leading bubble needs to rise to certain height such that the wake effect of leading bubble doesn't influence the trailing bubble formation. They reported that the leading bubble should rise a height of $1.7De$ for the wake effect to disappear. Where $De = 2(3V_{B,1}/(4\pi))^{1/3}$ and $V_{B,1}$ is the volume of the leading bubble. Approximating the terminal velocity of the bubble by $u_T = (2.14\ \sigma/\rho_l\ De + 0.505gDe)^{0.5}$ and equating

$$T_2 = T_{1,rise} = 1.7De/\ u_T \tag{4-3}$$

a critical formation period T_c related to the critical bubble volume $V_{B,c} = V_{B,1} = V_{B,2}$ is calculated. The critical bubble volume is equal to both bubble volumes at the instant of transition. If the bubble detachment time $t^* > T_c$, single periodic formation is expected because the leading bubble has moved to suitable height such that the wake effect is negligible and if $t^* < T_c$, double periodic formation is expected.

In a single periodic regime, the bubble formation is independent of interference with the previous bubble. Thus the detachment times are uniform, whereas in a double periodic regime the interference between the leading and trailing bubbles result in slight variation of detachment times. In double periodic regime no significant changes were observed during the formation of primary bubble. However the wake effect of leading bubble caused the trailing bubble to elongate in vertical direction during formation. This can be observed from Figure 4.16(b).

Varying the surface tension, increasing the flow rates are the two ways reported in literature [4] where a transition from periodic to double periodic can be observed. It has been reported [4] that at a flow rate of 200 ml/min, the transition from periodic to double periodic occurs when the density of liquid is increased from 1 to 1.25. However with present code, it is a bit difficult to handle higher flow rate problems (Q>150ml/min). So varying the surface tension was used to observe the double-periodic bubble formation. Numerical simulations were performed by varying the surface tension, keeping all the other parameters as constant. For the values of σ^{*}(= σ/ $\sigma_{ref)}$ at around 0.50, the phenomenon of double periodic bubble formation can be observed. If the surface tension is reduced, the volume of the bubble reduces. This causes an earlier detachment of the leading bubble. The wake effect of the leading bubble and the flow coming in causes the trailing bubble to detach earlier and rise in pairs. This is in good agreement with the results provided in literature [4]. Figure 4.16 shows both single periodic and double periodic bubble formation.

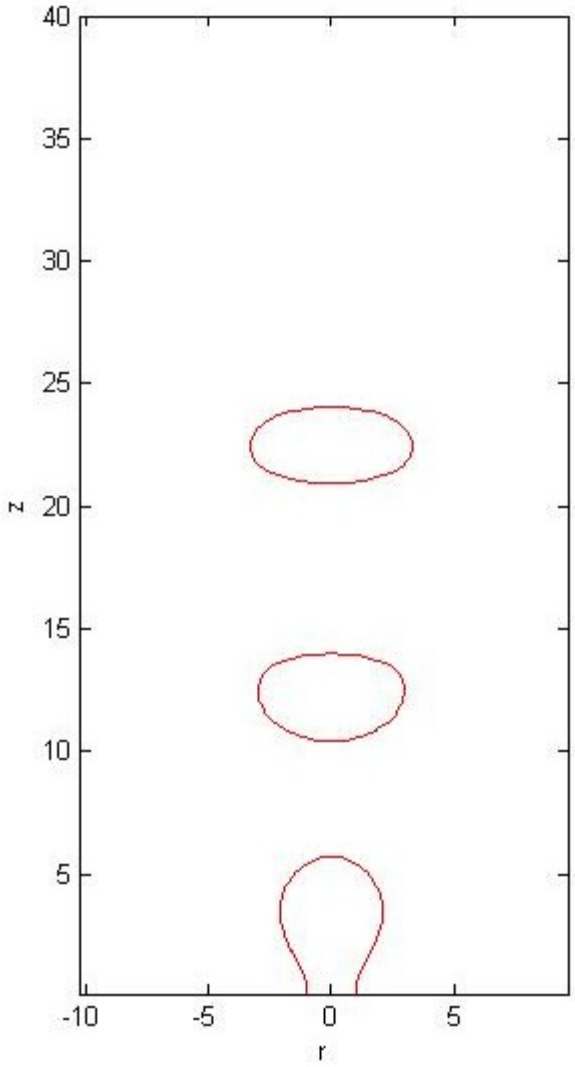

Figure 4.2 The schematic of bubble rising from an orifice

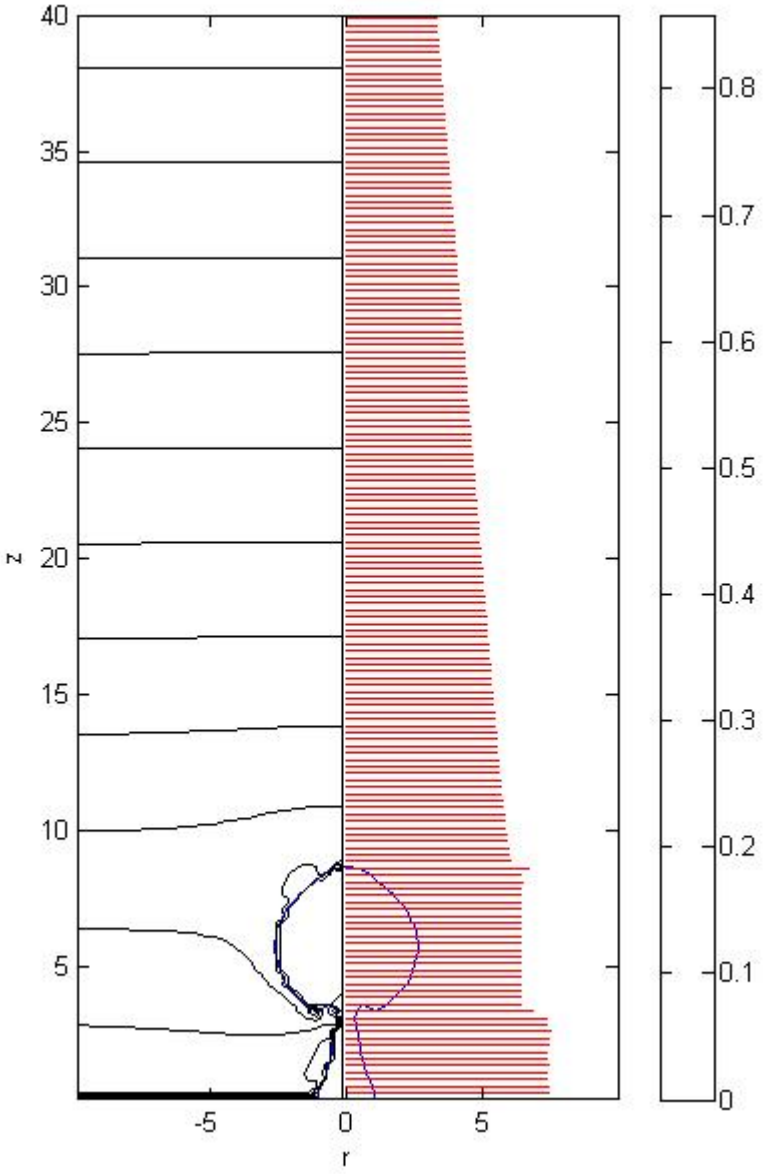

Figure 4.3 Bubble at the brink of pinch off: Pressure distribution
t = 41.82 ms

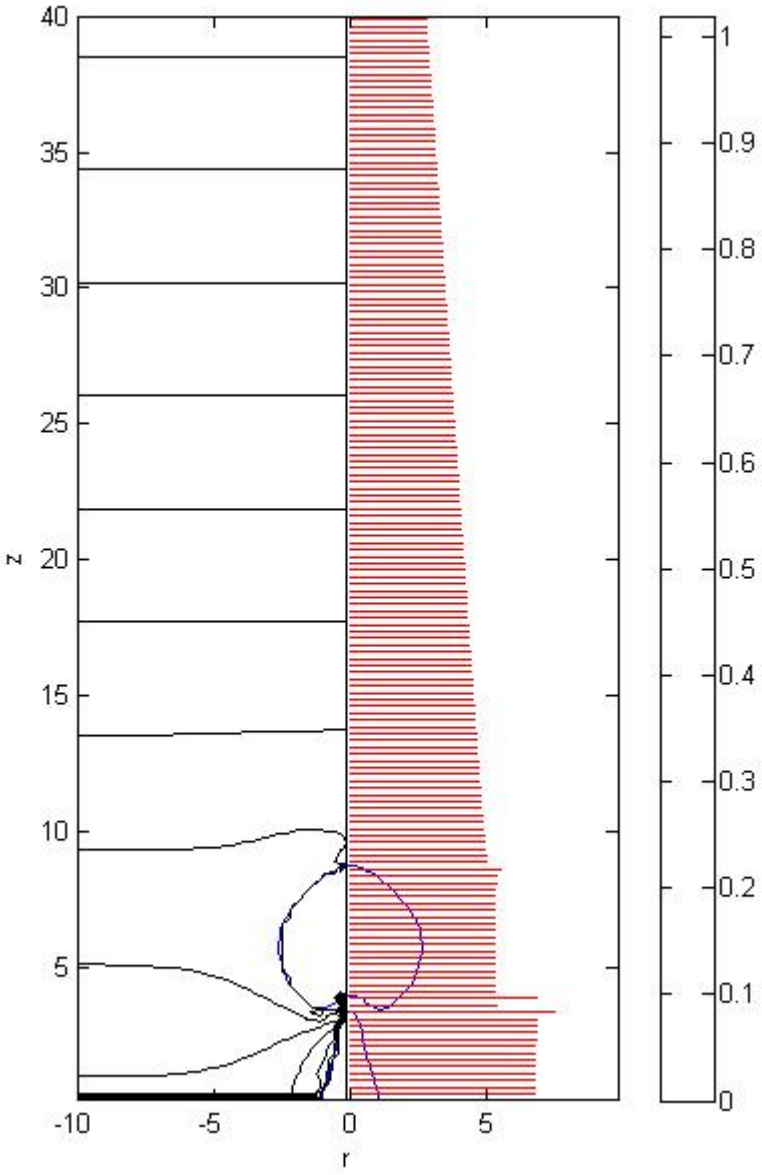

Figure 4.4 Bubble at the brink of pinch off: Pressure distribution
t = 41.99 ms

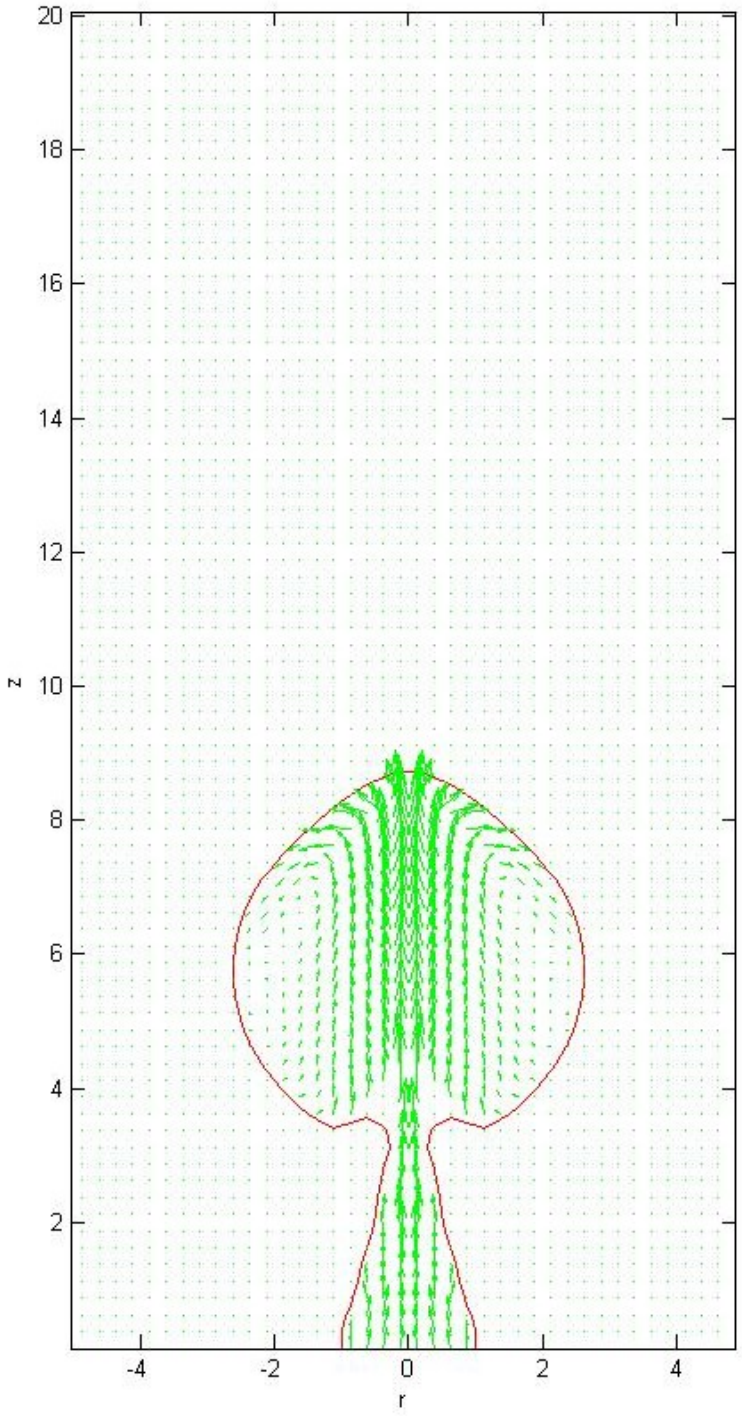

Figure 4.5 Velocity profile; t = 41.82 ms

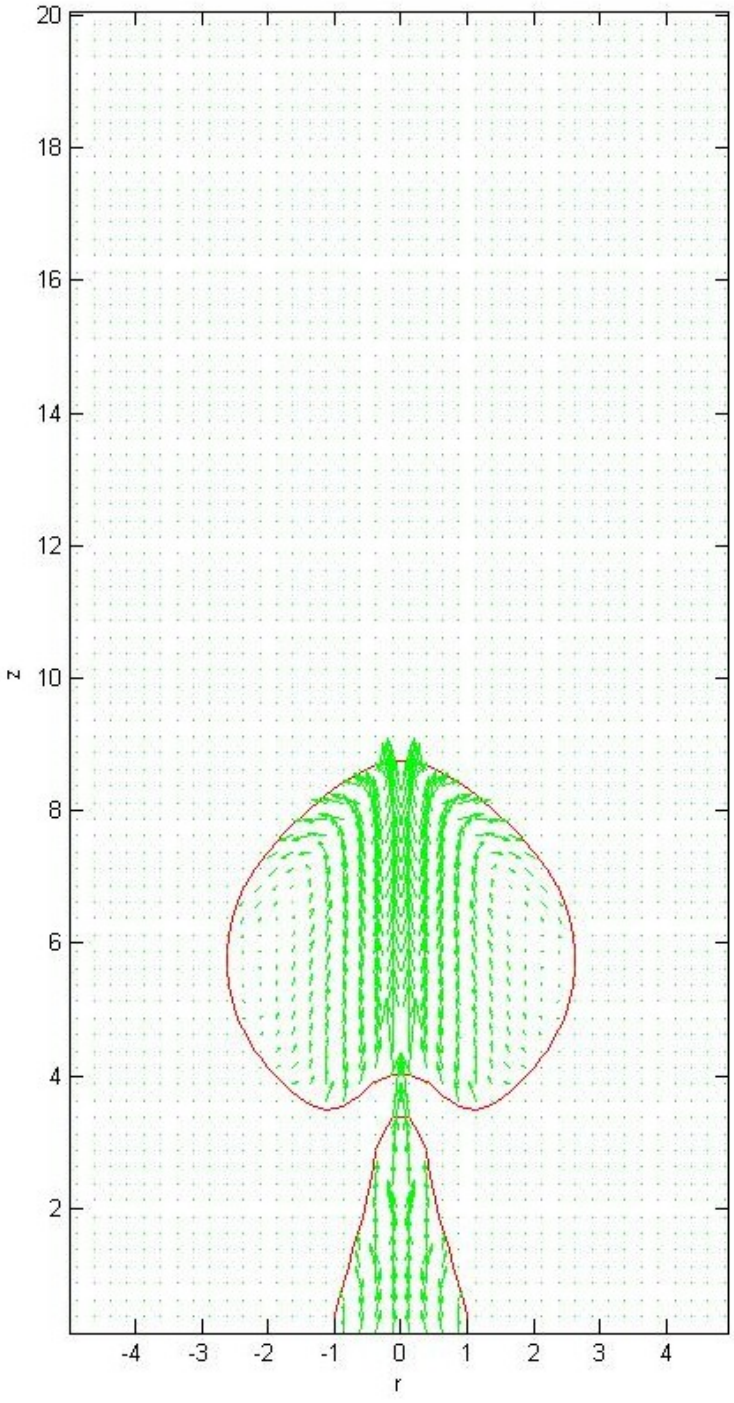

Figure 4.6 Velocity profile; t = 41.99 ms

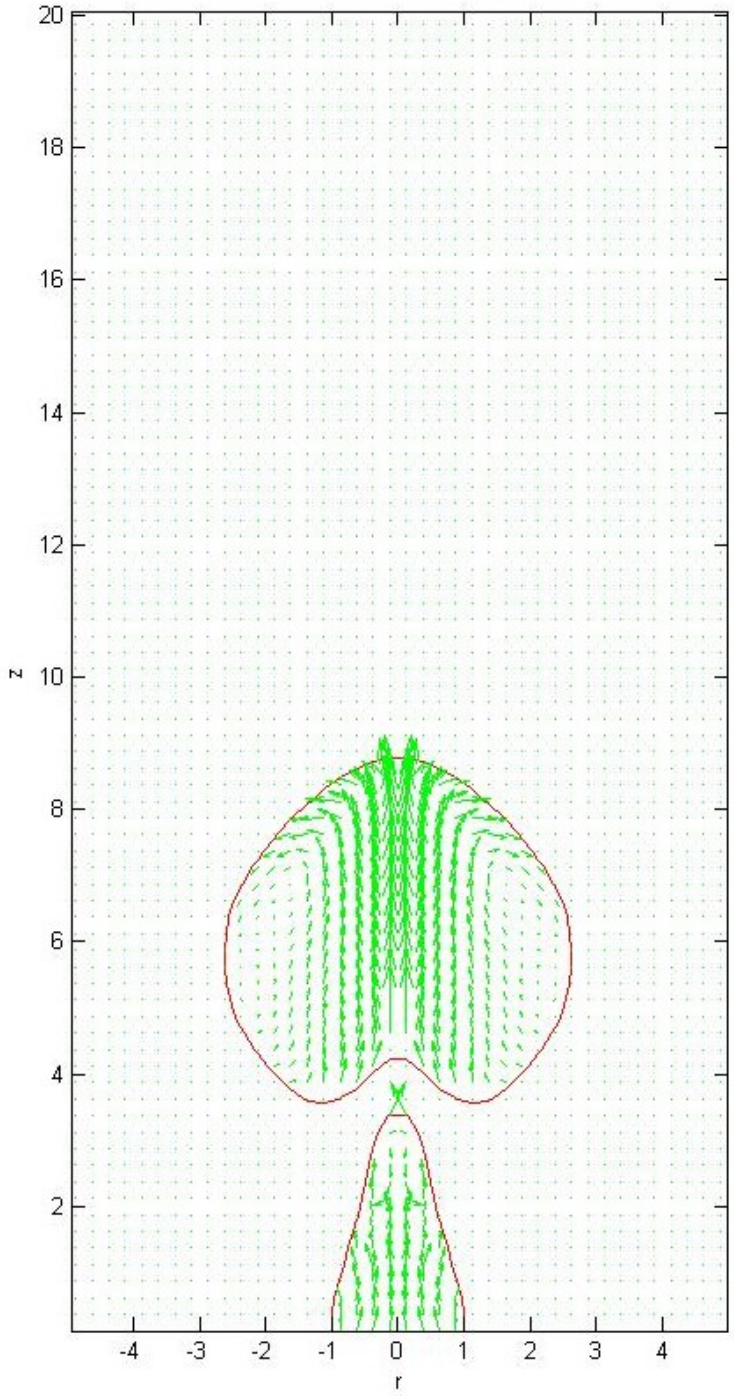

Figure 4.7 Velocity profile; t = 42.16 ms

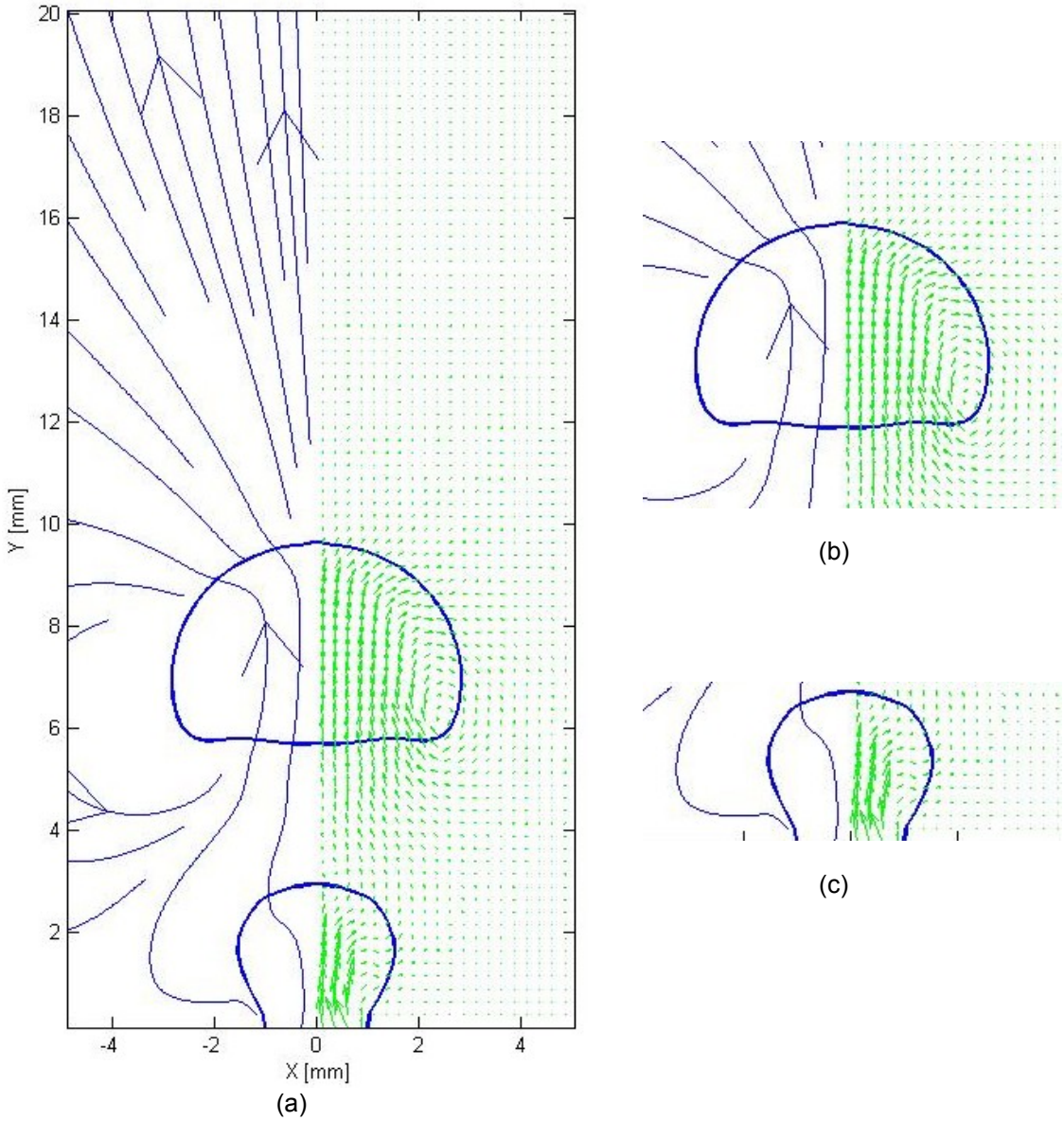

Figure 4.8 Bubble rising,(a) Velocity vector field and streamlines at one time instant,(b) Magnified view of leading bubble,(c) Magnified view of trailing bubble about to form

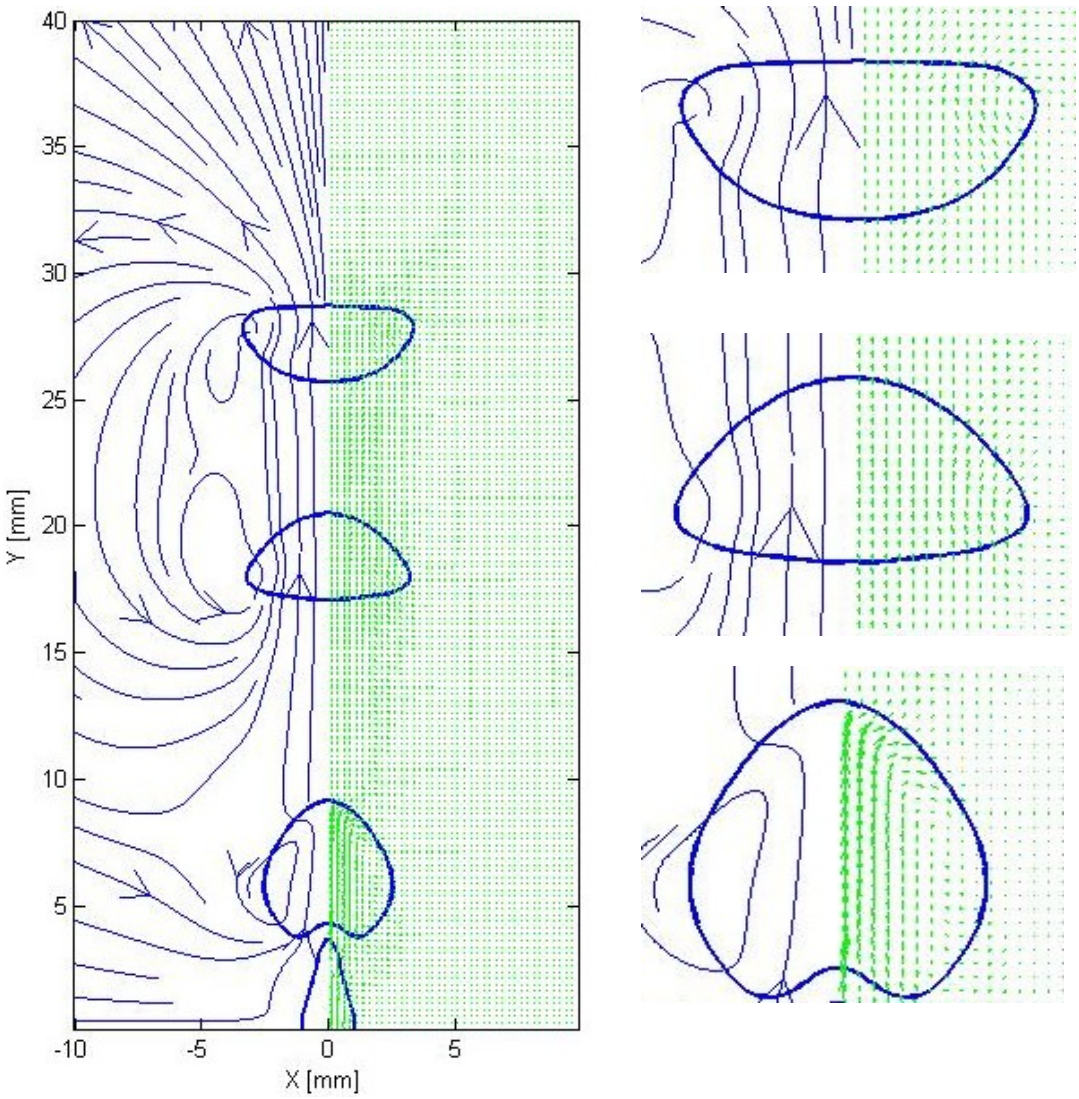

(a) (b)

Figure 4.9 Successive bubbles rising,(a) Velocity and stream line profiles,(b) Magnified view of each bubble

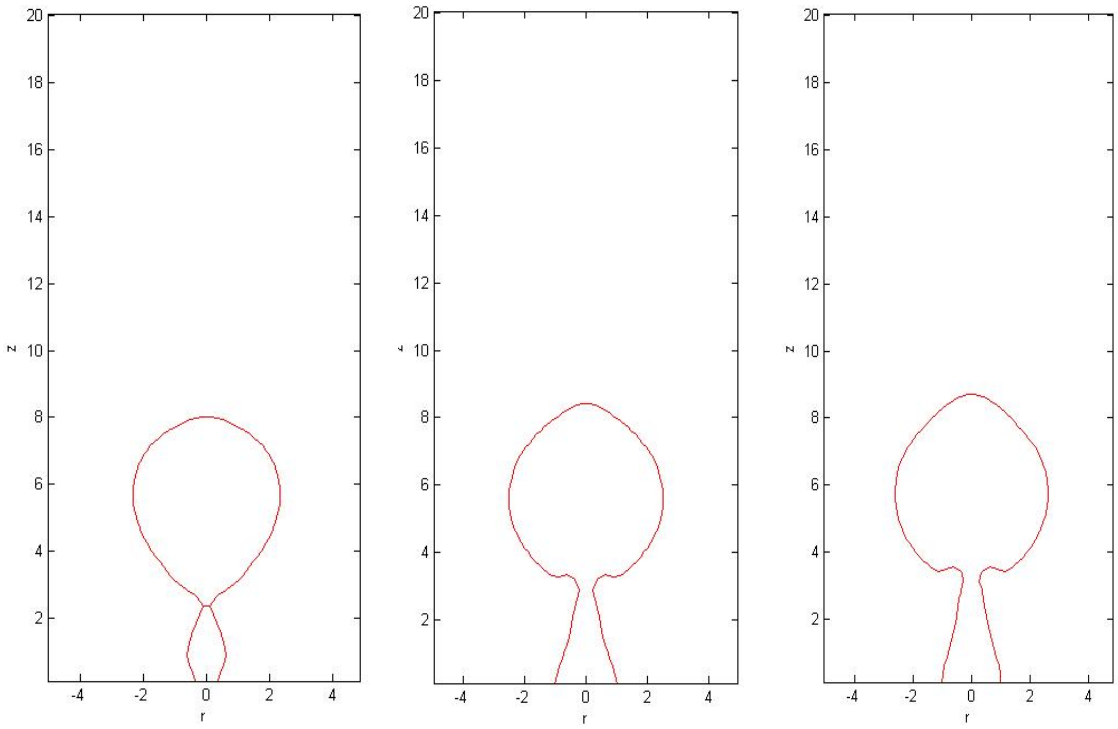

Figure 4.10 Evolution of bubbles with different flow rates, (a) Q = 50 ml/min, (b) Q = 80 ml/min, (c) Q = 100 ml/min

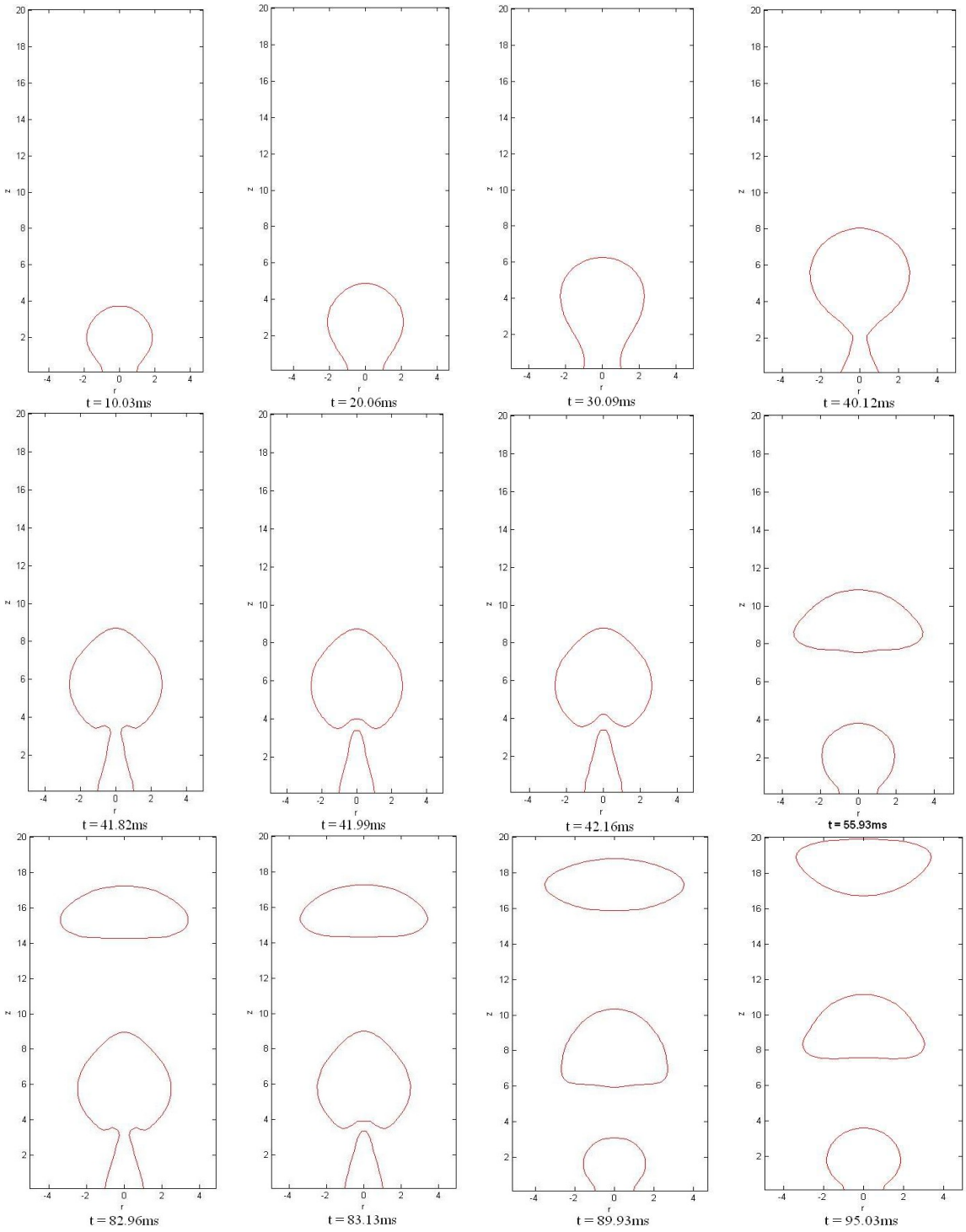

Figure 4.11 Bubble formation, detachment and ascendancy for a flow rate of 100 ml/min with 1 mm nozzle.

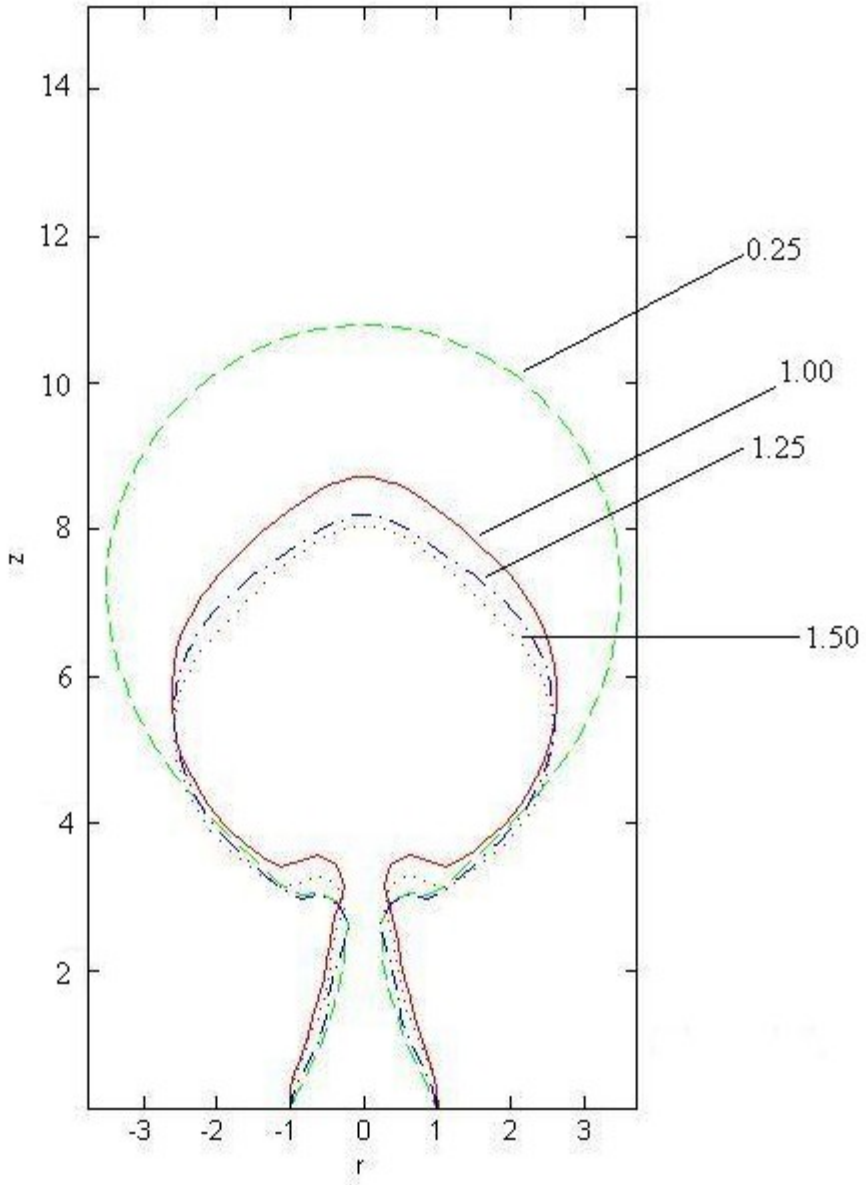

Figure 4.12 Bubble shapes for different densities overlapped

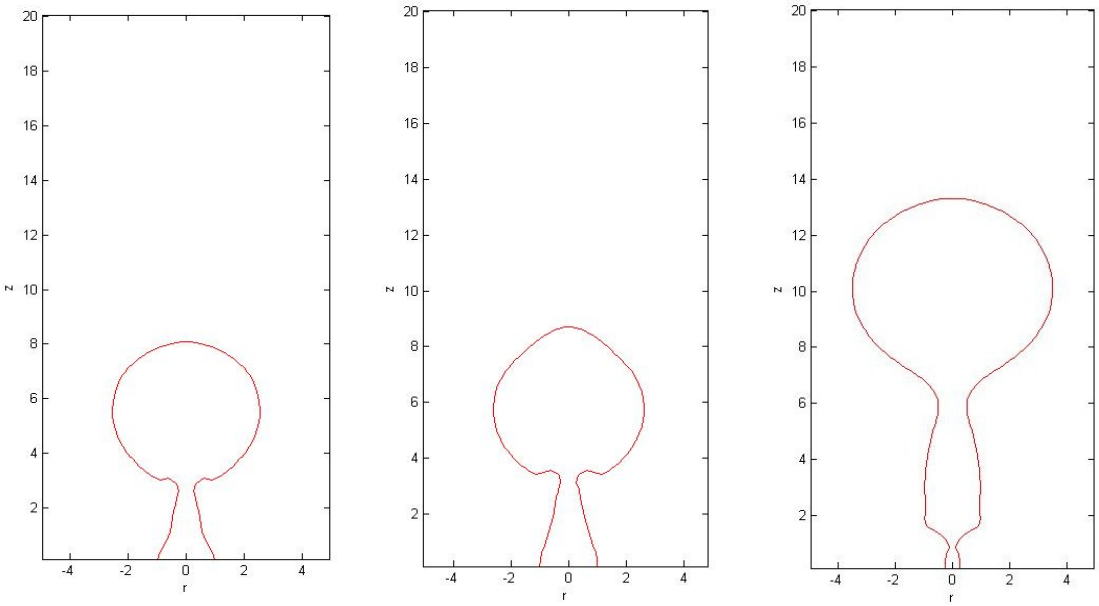

Figure 4.13 Effect of viscosity: Shape of bubbles at the brink of pinch off:
v/ v_{ref} = (a) 0.1, (b) 1.0, (c) 150

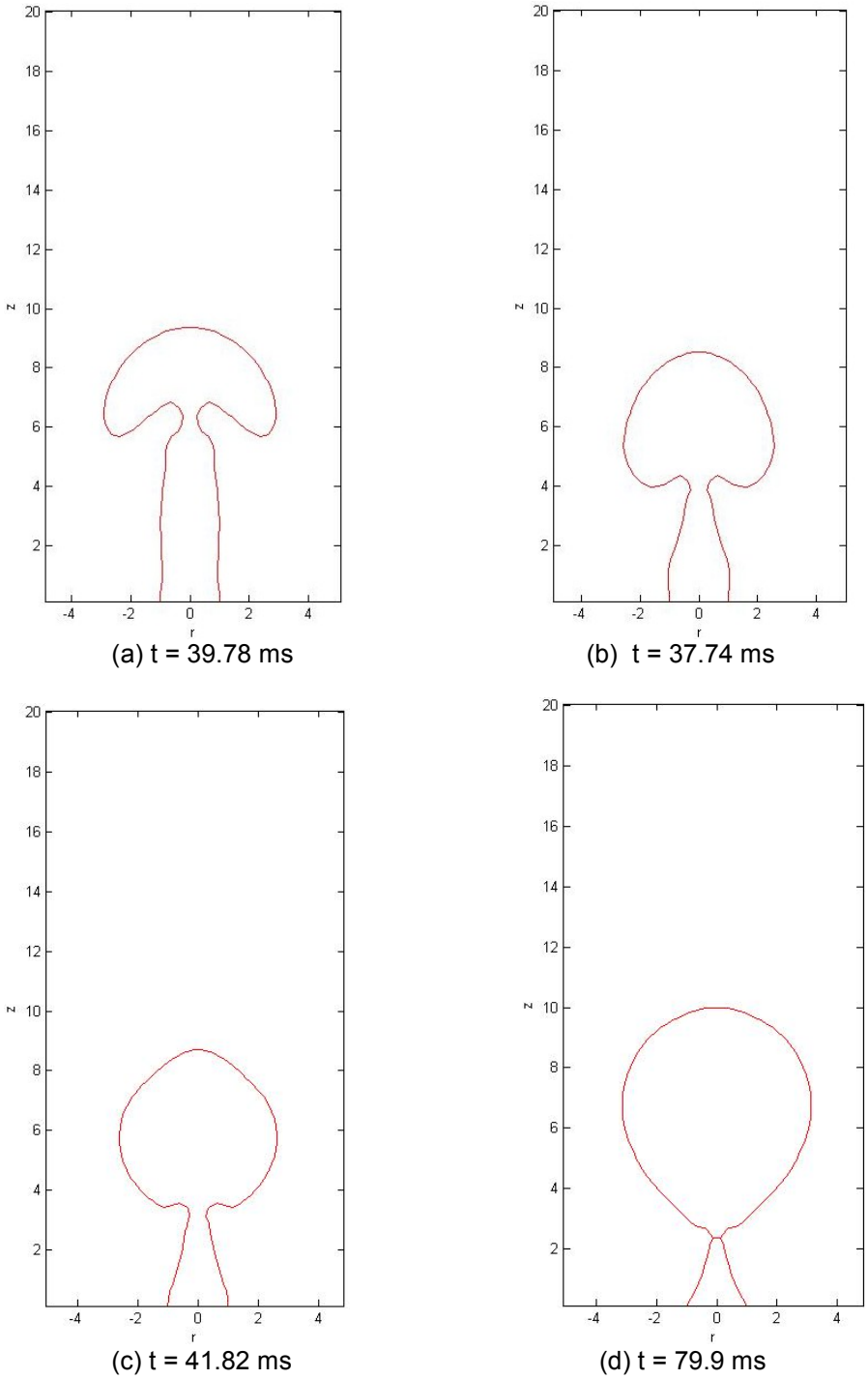

Figure 4.14 Shapes of bubbles for different surface tension coefficients
(a) σ/σ_{ref} = (a) 0.41, (b) 0.60, (c) 1.0, (d) 2.75

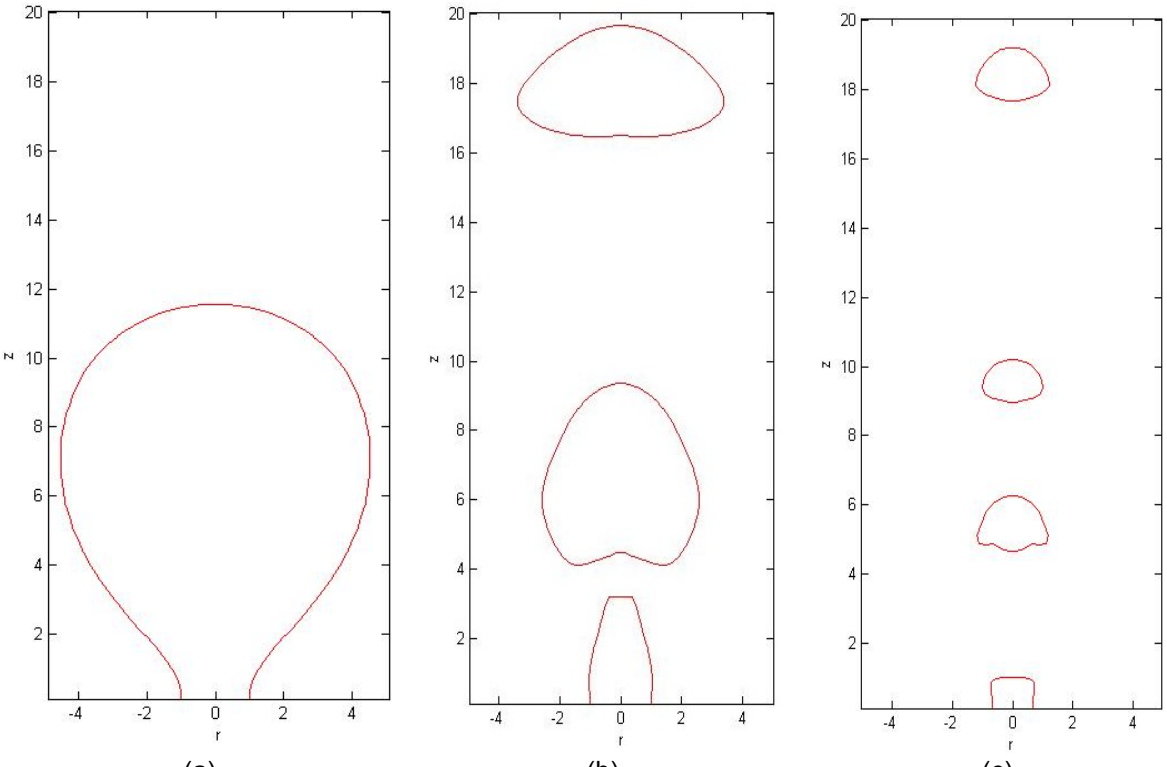

Figure 4.15 Sizes of bubbles for different gravity ratios at t = 254.8 ms
g / g_s= (a) 0.1, (b) 1.0, (c) 10.0

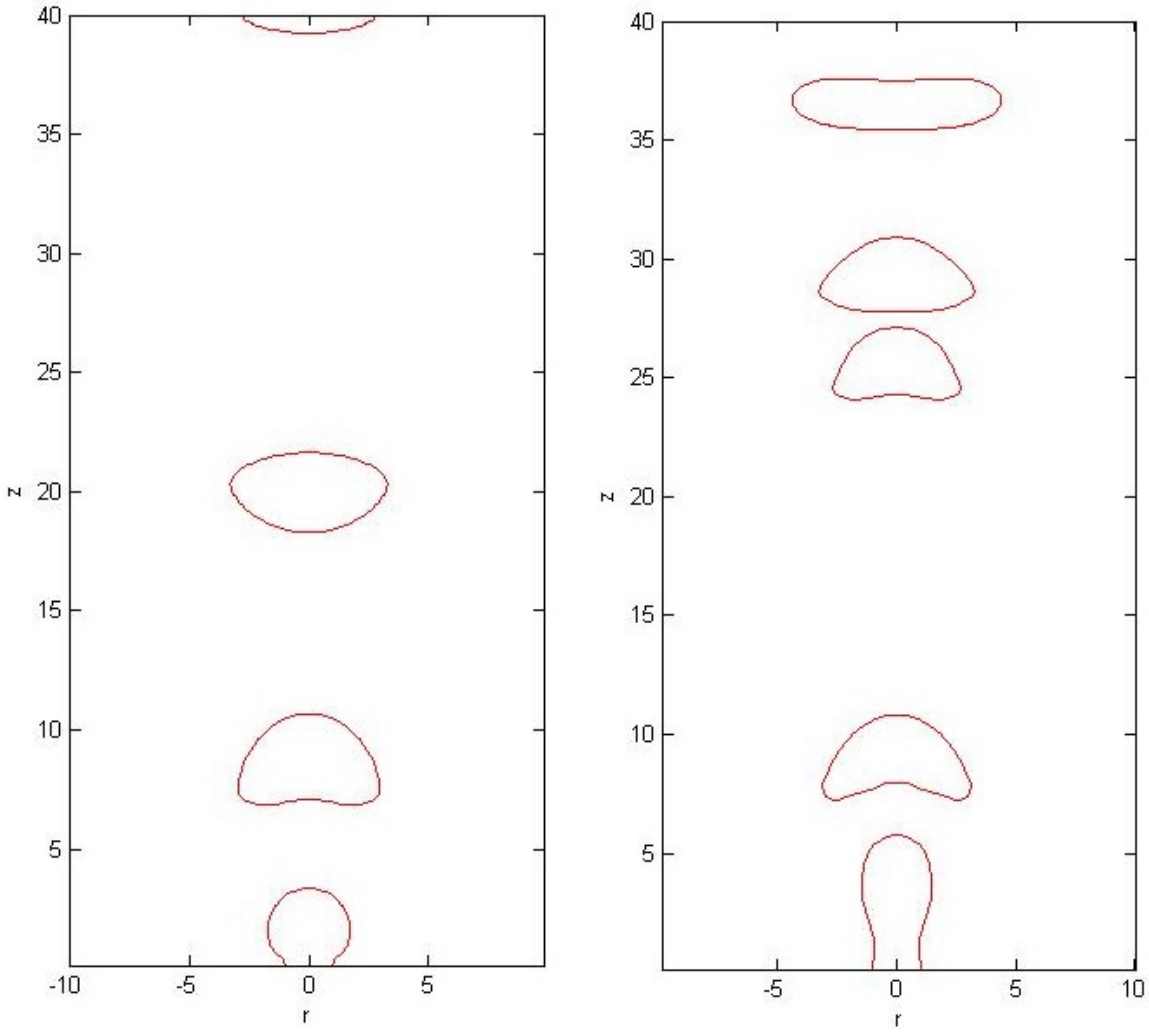

(a) (b)

Figure 4.16 Modes of bubble regimes: (a) single periodic regime
(b) double periodic regime

CHAPTER 5

CONCLUSIONS AND FUTURE WORK

The results obtained from numerical study of bubble formation at an orifice under constant inflow conditions were presented. The pressure boundary method has been applied for the numerical simulations. The influence of various operating conditions like orifice material, flow rate on the bubble formation was studied. The influence of different velocity profiles on bubble formation was also tested. It was observed that only a small time gap exists between detachment times of the uniform and parabolic velocity profiles. The study carried out used the radius of orifice as 1mm and the flow rate as 100 ml/min. Apart from these tests were also carried out to see the influence of fluid parameters. The phenomenon observed was that the bubble volume increases with decreasing density of the liquid. It can also be decreased if the either viscosity or surface tension is increased. The results obtained were compared with the results established in literature.

The results regarding transition from periodic to double-periodic have been observed and reported. In a double-periodic regime, the trailing bubble detaches a bit earlier as compared to a single-periodic regime. The reason for this would be the wake effect of the previous bubble. The volume of the trailing bubble has been observed to be smaller than regular. The double periodic regime was observed for surface tension coefficient values ranging from 0.45 to 0.55. It was also observed that in a periodic regime, after some time the second bubble coalesces with the leading bubble and move with a constant velocity.

Future study can be done in the areas by finding out a suitable method to solve the problems related to higher flow rates. A study about the effect of the width of the orifice on bubble formation can be done. Thickness of the orifice is a major factor in examining the effect of contact angle on the bubble formation. The present study can be extended to study the effect

of orifice material by defining a constant advancing and receding contact angles as provided in the literature [25]. In depth analysis about double-periodic study can be done to study the interaction between the bubble pairs. Apart from this the possibility of a triple-periodic bubble formation can also be examined.

APPENDIX A

CODE EXECUTION

In the present study FORTRAN was used as the programming language to write the program code under UNIX environment. The High Performance Computing (HPC) system at the University of Texas at Arlington was used to run the program code. In order to run a simulation four files namely the *input* file, the *file_nam.dat* file, the *bjob* file and the *ripple* code are to be placed in the same directory and then submitted to the queue at HPC. Of these four files *ripple* is the executable file. The *input* file contains information regarding problem geometry, initial conditions, fluid properties, numerical parameters etc. A sample *input* file is provided in Appendix B. The *file_nam.dat* file contains the number and names of output data and the *bjob* file contains the load sharing facility (LSF) instructions. While running the program, a data file is generated at regular intervals depending on the output frequency specified in the *input* file. The number of data files to be generated depends on the number specified by the user in the *file_nam.dat* file. If the program generates data files exceeding the number specified in the *file_nam.dat* file then the last file is overwritten until the computation is done.

The data file generated contains the solutions in a specified format which can be understood as: time, the first and last real cells in the r- and z-direction, location of the left side of each computational cell in the r-direction of the lower side of each computational cell in the z-direction, and the data containing the velocities in the r and z-directions, the volume fractions (VOF function value), the level set (LS) function value, the enthalpy, and the pressure. A sample output data file is provided in Appendix B.

MATLAB software was used to post process the data generated. This software enables us to analyze the data obtained in an efficient manner. Programs were written in MATLAB to generate the movies depicting bubble formation, to observe the velocity profiles, pressure distribution and streamline profiles. With the amount of features in it, MATLAB can be considered as user friendly and the suitable option to post process the data obtained.

APPENDIX B

SAMPLE INPUT AND OUTPUT

B.1 Sample INPUT

A sample *input* file is shown below. All the other parameters are taken over from a previous version of the code.

```
Injet Air Bubble[mm,ms,mg,K]
 $numparam
   alpha=2.0,
   autot=1.0,
   conserve=.false.,
   delt=1.0e-4,
   dtmax=8.28e-3,
   twfin=200000.0,
   con =0.3,
   fcvlim=0.5,
   idiv=1,
   dmpdt=300000000.0,
   prtdt=100000000.0,
   pltdt=1.7e-1,
   sym=.true.,
   kt=5,
   kb=6,
   kl=1,
   kr=2,
 $end
 $fldparam
   gy=-9.8e-3,
   icyl=1,
   isurf10=1,
   psat=0.0,
   pbc(2)=0.0,
   pbc(1)=0.5,
   xnug=1.005e-3,
   xnul=1.51e-2,
   rhofg=1.0,
   rhofl=1.2e-3,
   sigma=7.27e-2,
   vi=0.5305,
   vinf(1)=0.5305,
 $end
 $mesh
   nkx=1,
   xl = 0.0, 20.0,
   xc= 10.0,
   nxl = 40,
   nxr = 40,
   dxmn=0.25,
   nky=1,
   yl=0.0,80.0,
   yc=40.0,
```

```
 nyl=160,
 nyr=160,
 dymn=0.25,
$end
$obstcl
 nobs=4,
 ob1(1)=1.0, oc1(1)=-3.0, ioh(1)=1,
 oa1(2)=-1.0, oc1(2)=1.1, ioh(2)=0,
 ob1(3)=1.0, oc1(3)=-0.6, ioh(3)=1,
 oa1(4)=1.0, oc1(4)=-1.0, ioh(4)=0,
$end
$freesurf
 nfrsrf=3,iequib=0,
 fc1(1)=-1.0, ifh(1)=1,
 fb1(2)=1.0,fc1(2)=-3.0,ifh(2)=0,
 fa1(3)=-1.0,fc1(3)=1.0,ifh(3)=1,
$end
$graphics
 plots=.true., dump=.false.,
 iout = 0, 1, 0, 0, 0, 0, 0, 0, 0, 0, 0, 0, 0,
        0, 0, 0, 0, 0, 0, 0, 4, 8, 0, 0, 0, 0,
        0, 0, 0, 0, 0, 0, 0, 1, 0, 1, 1, 0, 1,
 iysymplt=1,
$end
$heateq
 heat = .false.,
 ischeme = 3,
 tid = 525.0,
 tip = 300.0,
 tia = 100.0,
 cpp = 227.0,
 cpd = 227.0,
 cpa = 50.0,
 tkp = 432.2,
 tkd = 67.0,
 lhpc = 58900.0,
 hmr = 5.0,
 tl = 510.0,
 ts = 505.0,
 teps = 1.0e-8,
$end
$coupled
 lsvof=.true.,
 ls = .false.,
$end
```

B.2 Sample OUTPUT

A sample output file and its explanations are given below.

```
1.59808E+001  <----- time
2, 80         <----- 1st real cell, last real cell in r-direction
2,320          <----- 1st real cell, last real cell in z-direction
0.00000E+000   <----- location of the left side of each computational cell in
2.50000E-001          the r-direction
5.00000E-001
7.50000E-001
1.00000E+000
1.25000E+000
1.50000E+000
1.75000E+000
2.00000E+000
.
.
.
.
.
0.00000E+000   <----- location of the left side of each computational cell in
2.50000E-001          the z-direction
5.00000E-001
7.50000E-001
1.00000E+000
1.25000E+000
1.50000E+000
1.75000E+000
2.00000E+000
.
.
.
.
.
0.00000E+000, 5.00000E-001, 0.00000E+000, 3.62108E-001, 0.00000E+000, 0.00000E+000
0.00000E+000, 5.00000E-001, 0.00000E+000, 5.77638E-001, 0.00000E+000, 0.00000E+000
0.00000E+000, 5.00000E-001, 0.00000E+000, 7.71898E-001, 0.00000E+000, 0.00000E+000
0.00000E+000, 5.00000E-001, 0.00000E+000, 9.64362E-001, 0.00000E+000, 0.00000E+000
0.00000E+000, 5.00000E-001, 0.00000E+000, 1.15691E+000, 0.00000E+000, 0.00000E+000
  (comp. 1)       (comp. 2)       (comp. 3)       (comp. 4)       (comp. 5)       (comp. 6)
```

In the above six-column matrix, components from comp.1 to comp.6 show the following solutions:

comp.1: velocity component in r-direction

comp.2: velocity component in z-direction

comp.3: VOF function value

comp.4: LS function value

comp.5: enthalpy

comp.6: pressure.

Detailed information about variables in the input file can be obtained from [1, 15, 27, 28].

REFERENCES

[1] Kothe, D. B., Mjolsness, R. C. and Torrey, M. D., “RIPPLE: A Computer Program for Incompressible Flows with Free Surfaces", Tech Report. LA-12007-MS (1994).

[2] Manasseh, R., Yoshida, S. & Rudman, M.“Bubble formation processes and bubble acoustic signals,” *Proc. 3rd Int. Conf. on Multiphase Flow (ICMF'98), Lyon, France,* paper 202 (*8–12 June 1998)*.

[3] Zhang, L., Shoji, M., “Aperiodic bubble formation from a submerged orifice,” Chemical Engineering Science 56, pp.5371-5381 (2001).

[4] Gerlach, D., Alleborn, N., Buwa, V., Durst, F., “Numerical simulation of periodic bubble formation at a submerged orifice with constant gas flow rate,” Chemical Engineering Science 62 pp. 2109-2125 (2007).

[5] Kumar, R., Kuloor, N.R., “The formation of bubbles and drops,” Advances in Chemical Engineering 8, pp.256-368 (1970).

[6] Clift, R., Grace, J.R., and Weber, M. E., Bubbles, Drops, and Particles. Academic Press, New York (1978).

[7] Tsuge, H., Hydrodynamics of bubble formation from submerged orifices. Encyclopedia of Fluid Mechanics 3, pp.191-232 (1986).

[8] Kulkarni, A.A., Joshi, J. B., “Bubble formation and bubble rise velocity in gas-liquid systems: a review. Industrial Engineering Chemistry Research,” 44, pp.5873-5931 (2005).

[9] Longuet-Higgins, M.S., Kerman, B.R., Lunde, K., ”The release of air bubbles from an underwater nozzle,” Journal of Fluid Mechanics 230, pp.365-390 (1991).

[10] Davidson, J. F., Schuler, B.O.G., Bubble formation at an orifice in a inviscous liquid. Transactions of the Institute of Chemical Engineers 38, pp.335-342 (1960a).

[11] Davidson, J. F., Schuler, B.O.G., Bubble formation at an orifice in a viscous liquid. Transactions of the Institute of Chemical Engineers 38, pp.144-154 (1960b).

[12] Kyriakides, N.K., Kastrinakis, E.G., Nychas, S.G., Goulas, A., "Bubbling from nozzles submerged in water: transition between bubbling regimes," Canadian Journal of Chemical Engineering 75, pp.684-691 (1997).

[13] Tufaile, A., Sartorelli, J.C., Bubble and spherical air shell formation dynamics. Physical Review E 66, 056204 (2002).

[14] Kim, I., Kamotani, Y., & Ostrach, S., "Modeling bubble and drop formation in flowing liquid in microgravity," A.I.Ch.E. Journal, 40, pp. 19-28 (1994).

[15] Mu-Chen, Lu, "Numerical Modeling of Multi-Phase Surface Flow," Ph.D. thesis, The University of Texas at Arlington (2000).

[16] Shyy, W., Udaykumar, H. S., Rao, M. M., and Smith, R. W., Computational Fluid Dynamics with Moving Boundaries, Taylor & Francis (1996).

[17] Hirt, C. W. and Nichols, B. D., "Volume of Fluid (VOF) Method for the Dynamics of Free Boundaries," Journal of Computational Physics, Vol. 39, pp. 201-225 (1981).

[18] Rudman, M., "Volume-Tracking Methods for Interfacial Flow Calculations," International Journal for Numerical Methods in Fluids, Vol. 24, pp. 671-691 (1997).

[19] Rudman, M., "A Volume-Tracking Method for Incompressible Multifluid Flows with Large Density Variations," International Journal for Numerical Methods in Fluids, Vol. 28., pp. 357-378 (1998).

[20] Sussman, M., Smereka, P. and Osher, S., "A level set approach for computing solutions to incompressible two-phase flow," *J. Comp. Phys.,* Vol. 114*,* pp. 146-154 (1994).

[21] A. Y. Tong and Z. Wang., "A Numerical Method for Capillarity-Dominant Free Surface Flows," Journal of Computational Physics, Vol. 221, pp. 506-523 (2007).

[22] Kang, M., Fedkiw, R. and Liu, X.-D., “A Boundary Condition Capturing Method for Multiphase Incompressible Flow,” *J. Sci. Comput.,* Vol. 15, pp. 323-360 (2000).

[23] Gibou, F., Fedkiw, R., Cheng, L. T. and Kang, M., “A second order accurate symmetric discretization of the Poisson equation on irregular domains,” *J. Comput. Phys.,* Vol. 176, pp. 205-227 (2002).

[24] Kershaw, D. S., “The Incomplete Cholesky-Conjugate Gradient Method for the Iterative Solution of Systems of Linear Equations,” *Journal of Computational Physics*, Vol. 26, pp. 43-65 (1978).

[25] Abhijit Mukherjee and Satish G. Kandlikar., “Numerical study of single bubbles with dynamic contact angle during nucleate pool boiling,” International Journal of Heat and Mass Transfer, v 50, n 1-2, p 127-138 (January 2007).

[26] Wong, H., Rumschitzki, D., Maldarelli, C., “Theory and experiment on the low-Reynolds-number expansion and contraction of a bubble pinned at a submerged tube tip,” Journal of Fluid Mechanics 356, pp. 93-124 (1998).

[27] Ryohei Kamiya, “A Numerical study of pendant drop formation from a capillary tube,” Master’s thesis, The University of Texas at Arlington (2005).

[28] Wang, Z., “Numerical study on capillary-dominant free surface and interfacial flows,” Ph.D. Dissertation, Department of Mechanical and Aerospace Engineering, The University of Texas at Arlington, TX (2006).

BIOGRAPHICAL INFORMATION

Sheshi Kumar Takkallapally received his Bachelor's degree in Mechanical Engineering from Balaji Institute of Technology and science, JNT University, INDIA, in May 2006. He received his Master's degree in Mechanical Engineering from The University of Texas at Arlington in December 2009. His area of interest includes fluid dynamics, design, and thermal sciences.